J. Fluid Mech. (1988), *vol.* 195, *pp.* 77–111
Printed in Great Britain

Growth and decay of turbulence in a stably stratified shear flow

By J. J. ROHR†, E. C. ITSWEIRE‡, K. N. HELLAND§‖ AND C. W. VAN ATTA¶‖

† Naval Ocean Systems Center, Code 634, San Diego, CA 92152, USA

‡ Chesapeake Bay Institute, The Johns Hopkins University, Baltimore, MD 21211, USA

‖ Department of Applied Mechanics and Engineering Sciences, University of California, San Diego, La Jolla, CA 92093, USA

§ Data Ready, Suite 150 4647T, Highway 280 East, Birmingham, AL 35243, USA

¶ Scripps Institution of Oceanography, University of California, San Diego, CA 92093, USA

The behaviour of an evolving, stably stratified turbulent shear flow was investigated in a ten-layer, closed-loop, salt-stratified water channel. Simultaneous single-point measurements of the mean and fluctuating density and longitudinal and vertical velocities were made over a wide range of downstream positions. For strong stability, i.e. a mean gradient Richardson number R_i greater than a critical value of $R_{i_{cr}} \approx 0.25$, there is no observed growth of turbulence and the buoyancy effects are similar to those in the unsheared experiments of Stillinger, Helland & Van Atta (1983) and Itsweire, Helland & Van Atta (1986). For values of Richardson number less than $R_{i_{cr}}$ the turbulence grows at a rate depending on R_i and for large evolution times the ratio between the Ozmidov and turbulent lengthscale approaches a constant value which is also a function of Richardson number.

Normalized velocity and density power spectra for the present experiments conform to normalized spectra from previous moderate- to high-Reynolds-number studies. With increasing $\tau = (x/\bar{U})(\partial\bar{U}/\partial z)$ or decreasing stability, the stratified shear spectra exhibit greater portions of the universal non-stratified spectrum curve. The shapes of the shear-stress and buoyancy-flux cospectra confirm that they act as sources and sinks for the velocity and density fluctuations.

1. Introduction

In the earliest studies of unstratified, uniform-gradient shear flows the turbulent kinetic energy was observed after an initial decay to approach a constant level downstream (see Rose 1966, 1970; Champagne, Harris & Corrsin 1970, hereinafter referred to as CHC; Mulhearn & Luxton 1975). The apparent constant level of the turbulent kinetic energy was later found to be a result of insufficient wind-tunnel length for the values of applied shear. The dimensionless development time $\tau = (x/\bar{U})(\partial\bar{U}/\partial z)$ did not exceed 3.6 in these experiments. Growth of the turbulent kinetic energy was first observed by Harris, Graham & Corrsin (1977, hereinafter referred to as HGC) for τ exceeding 4. This was later corroborated by Tavoularis & Corrsin (1981, hereinafter referred to as TC) in an experiment where they superimposed a passive scalar (weak temperature gradient) on the same velocity field.

Earlier, Webster (1964) had succeeded in generating an actively stratified shear flow in a wind tunnel using temperature to produce buoyancy effects. At 1.73 and 4.57 m downstream of the shear generating grid, Webster measured turbulent

diffusivities, kinetic energies and lengthscales as a function of the gradient Richardson number $R_i = N^2/(\partial\bar{U}/\partial z)^2$, where $N^2 = -(g/\bar{\rho})(\partial\bar{\rho}/\partial z)$. Unfortunately, Webster found a different dependence on R_i at each position, which he attributed to the flow not reaching a 'steady state'. The mean velocity shear of Webster was produced by a grid of unequal-diameter bars. A rough estimate of the resulting τ associated with Webster's grid can be obtained from the formula of Owen & Zienkiewicz (1957):

$$\bar{U}(z) = \bar{U}_C[1 + 0.85(z/h - \tfrac{1}{2})],$$

where $\bar{U}(z)$ is the average velocity at the height z measured from the tunnel floor, $\bar{U}_C$ is the centreline velocity and h the height of the tunnel. This formula predicts $\tau \approx 3$ and 7 at the respective measuring positions of 1.73 and 4.57 m downstream of the grid. Apparently the measurements at the first position ($\tau < 4$) were still in the region of decaying turbulence behind the shear generating grid. The present study was designed to investigate how, as a function of R_i, the turbulent kinetic energy grows or decays downstream beyond the initial influence of the grid. The unstratified-shear experiments of Rohr *et al.* (1988, hereinafter referred to as RIHV) had values of τ exceeding 4 and as expected distinct growth in the turbulence was observed, occurring first around $\tau = 4.5$.† By repeating these measurements with different density gradients the effect of buoyancy on the evolution of turbulence in a uniform mean shear could be investigated.

Section 2 briefly describes the experimental facility and instrumentation. Relevant dynamical equations, lengthscales and dimensionless parameters are presented in §3. The behaviour of the turbulent kinetic energy, turbulent production and buoyancy flux is investigated in §4.1 for different values of Richardson number and development time τ. Section 4.2 compares the present evolution of turbulent lengthscales with other laboratory stratified-shear-flow measurements, as well as the unsheared stratified experiments of Stillinger, Helland & Van Atta (1983) and Itsweire, Helland & Van Atta (1986) (hereinafter referred to as SHV and IHV respectively). Section 5 investigates the general behaviour of the velocity and density spectra. Section 6 discusses possible similarities with oceanographic data and finally, §7 contains the concluding remarks.

2. Experimental facility

The UCSD ten-layer, closed-loop water channel was designed to produce stably stratified, turbulent shear flows in which measurements could be extended sufficiently far downstream to study evolving turbulence statistics. The basic facility has been described in detail by Stillinger *et al.* (1983).

Two different inlet configurations were employed in the present study. The first one was identical to that of SHV and IHV, thereby providing the opportunity for direct comparison with their unsheared stratified measurements. The second inlet configuration employed consisted of the diffuser section described by RIHV. With the diffuser section in place it was found that the desired mean velocity profile was maintained much further downstream. With either inlet section, the velocity profile was observed to be time independent and decayed slowly over the range of downstream measuring positions. The density gradient was observed to decrease

† It should be noted that for the measurements of Karnik & Tavoularis (1983) taken behind grids separated from the inlet by relatively large values of τ, the growth of the turbulence around $\tau = 4$ (τ origin taken at the grid) was not observed (see RIHV).

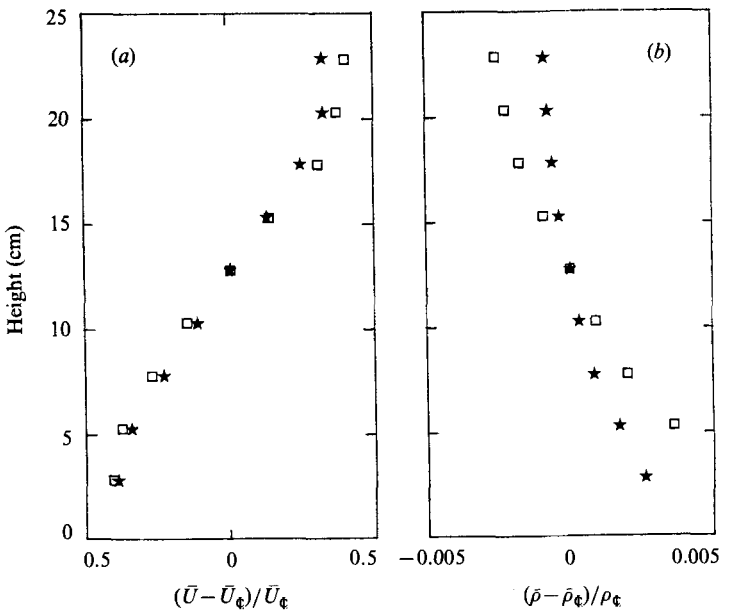

FIGURE 1. Vertical velocity (*a*) and density (*b*) profiles without diffuser (same inlet conditions as SHV and IHV). □, $x/M = 20$; ★, $x/M = 70$ (30 min later).

over time, but at a rate slow enough that the turbulent density and velocity fields at a point were nearly statistically stationary over each period of data averaging. Figures 1 and 2 compare typical mean velocity and density profiles at two downstream locations for both configurations.

The instrumentation was the same as that used by SHV and IHV. Standard quartz-coated TSI films mounted on an X-film probe provided measurements of the downstream ($\bar{U}, u$) and vertical velocity (w) components. Using the error analysis of Stillinger (1983) the salinity contamination of the measured velocity components was found to be negligible and the low-frequency temperature drift was compensated for with temperature measurements from a platinum resistance thermometer. A four-wire conductivity probe, having both good spatial resolution (<2.5 mm) and very low drift, developed by Head (1983), measured the local instantaneous conductivity of the salt solution. The instantaneous conductivity was then converted into an instantaneous density ($\bar{\rho}, \rho$). Earlier work by Stillinger (1981), where the magnitude of the density fluctuations were comparable with those of the present investigation, showed that the conductivity probe resolved at least 90% of the density variance but could not resolve the scalar dissipation rate. The centre-to-centre separation between the conductivity and X-film probes was small enough (<1 mm) to measure accurately the buoyancy flux $(g/\bar{\rho})(\overline{\rho w})$ without correcting for sensor separation.

The turbulence statistics essential to this study which could be accurately estimated include the r.m.s. horizontal and vertical turbulent velocity fluctuations (u' and w', respectively), the r.m.s. density fluctuation (ρ') and the kinetic-energy dissipation rate (ϵ). The variances on estimates of the buoyancy flux $(g/\bar{\rho})(\overline{\rho w})$ and turbulent production $-\overline{uw}(\partial\bar{U}/\partial z)$ were found to be significantly larger. Longer averaging times are needed to determine the statistics of cross-moments (e.g. $\overline{uw}, \overline{\rho w}$) to the same accuracy as the variances (e.g. $\overline{u}^2, \overline{w}^2, \overline{\rho}^2$). In the water channel, record

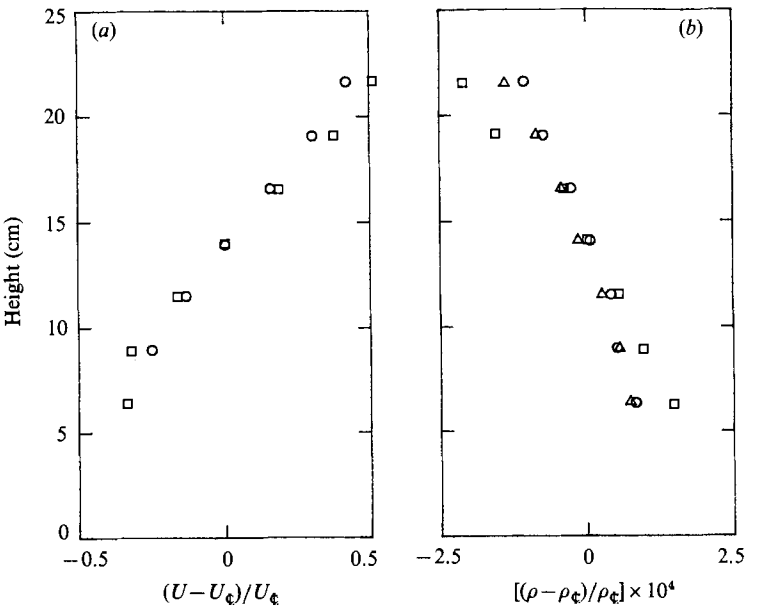

FIGURE 2. Vertical velocity (*a*) and density (*b*) profiles with diffuser. (*a*) □, $x/M = 20$; ○, $x/M = 160$. (*b*) Density profiles □, △, ○ were taken 30 min apart; by adding fresh and saturated salt water as needed the kink in the first profile (□) could be smoothed and the resulting profile (△) could be maintained (○).

lengths are limited by dissolved gases in the water coming out of solution and forming bubbles on the heated films (see Stillinger 1981). Generally the films were operated at about 12 °C above the ambient fluid temperatures and periodically swept clean by a jet of air, allowing between 10 and 16 s of continuous uncontaminated data. The total number of records is limited by the slowly decaying density profile.

The density profile decays in time because the water is recirculated and, therefore, measurements taken at later times are associated with smaller mean density gradients. The decrease of the density gradient for the first set of experiments, with the same inlet configuration as SHV (see figure 1), is found to be relatively fast. In these cases, the faster decay of the downstream velocity gradient increased mixing. For the second set of experiments, which incorporated the diffuser of RIHV, the decay of both the velocity and density profiles is significantly reduced (see figure 2). For either set of measurements, the density profile changes most rapidly with downstream distance in the upper part of the water channel where the local mean velocities are the largest. All detailed turbulence measurements were taken at the midpoint of the channel where downstream changes in $\partial\bar{U}/\partial z$, $\partial\bar{U}/\partial y$ (nearly zero), and $\partial\bar{\rho}/\partial z$ are smallest. There the turbulent lengthscale, as measured by $L_t = -\rho'/(\partial\bar{\rho}/\partial z)$, always remained at least several times smaller than the extent of the linear part of the accompanying velocity and density gradients. The corresponding transverse (y) mean velocity and density profiles were observed (Rohr 1985) to be uniform over distances at least as great as the linear part of the vertical mean velocity and density gradients.

3. Theoretical background

3.1. *Dynamical equations*

The flow is assumed to be incompressible, steady and transversely homogeneous. The density fluctuations are small compared with the mean density so that the Boussinesq approximation can be invoked. The general equations for the individual components of the fluctuating kinetic energy reduce to

$$\bar{U}\frac{\partial\overline{u^2}}{\partial x}+2\overline{uw}\frac{\partial\bar{U}}{\partial z}+\frac{\partial\overline{u^2w}}{\partial z}+\frac{\partial\overline{u^3}}{\partial x}=-\frac{2}{\bar{\rho}}\left(\frac{\partial}{\partial x}\overline{up}-\overline{p\frac{\partial u}{\partial x}}\right)-2\nu\left(\overline{\frac{\partial u}{\partial x_i}\frac{\partial u}{\partial x_i}}\right), \tag{1}$$

$$\bar{U}\frac{\partial\overline{v^2}}{\partial x}+\frac{\partial\overline{v^2u}}{\partial x}+\frac{\partial\overline{v^2w}}{\partial z}=-\frac{2}{\bar{\rho}}\left(\frac{\partial}{\partial y}\overline{vp}-\overline{p\frac{\partial v}{\partial y}}\right)-2\nu\left(\overline{\frac{\partial v}{\partial x_i}\frac{\partial v}{\partial x_i}}\right), \tag{2}$$

$$\bar{U}\frac{\partial\overline{w^2}}{\partial x}+\frac{\partial\overline{w^2u}}{\partial x}+\frac{\partial\overline{w^3}}{\partial z}=-\frac{2}{\bar{\rho}}\left(\frac{\partial}{\partial z}\overline{wp}-\overline{p\frac{\partial w}{\partial z}}\right)-2\frac{g}{\bar{\rho}}\overline{\rho w}-2\nu\left(\overline{\frac{\partial w}{\partial x_i}\frac{\partial w}{\partial x_i}}\right), \tag{3}$$

where $\bar{U}$ is the mean longitudinal velocity, u, v and w are the velocity fluctuations in the x-, y- and z-directions, respectively, $\bar{\rho}$ is the mean density, ρ is the density fluctuation, and ν is the kinematic viscosity. Production of kinetic energy only occurs in (1) for the u-component. The v- and w-components receive their energy through the pressure interaction terms.

Similarly the equations for the fluctuating potential energy, shear stress and buoyancy flux become respectively (e.g. Launder 1975)

$$\bar{U}\frac{\partial\overline{\rho^2}}{\partial x}+2\overline{\rho w}\frac{\partial\bar{\rho}}{\partial z}+\frac{\partial\overline{\rho^2u}}{\partial x}+\frac{\partial\overline{\rho^2w}}{\partial z}=-2D\left(\overline{\frac{\partial\rho}{\partial x_i}\frac{\partial\rho}{\partial x_i}}\right), \tag{4}$$

$$\bar{U}\frac{\partial\overline{uw}}{\partial x}+\overline{w^2}\frac{\partial\bar{U}}{\partial z}+\frac{\partial\overline{u^2w}}{\partial x}+\frac{\partial\overline{uw^2}}{\partial z}=-\frac{1}{\bar{\rho}}\left(\overline{u\frac{\partial p}{\partial x}}+\overline{w\frac{\partial p}{\partial z}}\right)-\frac{g}{\bar{\rho}}\overline{\rho u}-2\nu\left(\overline{\frac{\partial u}{\partial x_i}\frac{\partial w}{\partial x_i}}\right), \tag{5}$$

$$\bar{U}\frac{\partial\overline{\rho w}}{\partial x}+\overline{w^2}\frac{\partial\bar{\rho}}{\partial z}+\frac{\partial\overline{\rho w^2}}{\partial z}+\frac{\partial\overline{\rho uw}}{\partial x}=-\frac{1}{\bar{\rho}}\overline{\rho\frac{\partial p}{\partial z}}-\frac{g}{\bar{\rho}}\overline{\rho^2}-(\nu+D)\overline{\frac{\partial w}{\partial x_i}\frac{\partial\rho}{\partial x_i}}, \tag{6}$$

where D is the scalar diffusivity. Earlier experiments (HGC) implied that the triple correlations in (1), (2), (3) and (5) were nearly homogeneous in x and z when the flow was not stratified. If the same homogeneity also applies to $\overline{\rho^2u}$, $\overline{\rho^2w}$, $\overline{\rho uw}$, $\overline{\rho w^2}$ and the pressure–velocity and pressure–density correlation then (1)–(6) lead to

$$\bar{U}\frac{\partial(\frac{1}{2}\overline{q^2})}{\partial x}=-\overline{uw}\frac{\partial\bar{U}}{\partial z}-\frac{g}{\bar{\rho}}\overline{\rho w}-\epsilon, \tag{7}$$

$$\bar{U}\frac{\partial\overline{uw}}{\partial x}=-\overline{w^2}\frac{\partial\bar{U}}{\partial z}-\frac{g}{\rho}\overline{\rho u}, \tag{8}$$

$$\bar{U}\frac{\partial\frac{1}{2}\overline{\rho^2}}{\partial x}=-\overline{\rho w}\frac{\partial\bar{\rho}}{\partial z}-\chi, \tag{9}$$

$$\bar{U}\frac{\partial\overline{\rho w}}{\partial x}=-\overline{w^2}\frac{\partial\bar{\rho}}{\partial z}-\frac{g}{\bar{\rho}}\overline{\rho^2}, \tag{10}$$

where

$$\epsilon=\nu\left(\overline{\frac{\partial u_i}{\partial x_j}\frac{\partial u_i}{\partial x_j}}\right)$$

is the rate of dissipation of turbulent kinetic energy,

$$\chi = D\left(\overline{\frac{\partial \rho}{\partial x_i}\frac{\partial \rho}{\partial x_i}}\right)$$

is the rate of diffusive destruction of density fluctuations and $\overline{q^2} = \overline{u^2}+\overline{v^2}+\overline{w^2}$. Although pressure interaction terms do not appear explicitly in (7), this does not necessarily imply that as a result of the previous approximations there is no longer a mechanism for the redistribution of energy among the velocity components. For incompressible flow

$$\overline{p\frac{\partial u}{\partial x}}+\overline{p\frac{\partial v}{\partial y}}+\overline{p\frac{\partial w}{\partial x}} = 0,$$

therefore these pressure terms can exchange energy between the various components without appearing in (7), since when summed they do not change the total energy (Tennekes & Lumley 1972). Equations (7)–(10) can be rewritten in terms of turbulent kinetic energy

$$E_{\mathrm{K}} = \tfrac{1}{2}\overline{q^2},$$

turbulent production

$$P = -\overline{uw}\,\partial\bar{U}/\partial z,$$

fluctuating potential energy

$$E_{\mathrm{P}} = -\tfrac{1}{2}(g/\bar{\rho})\,\overline{\rho^2}/(\partial\bar{\rho}/\partial z)$$

and buoyancy flux

$$F_{\mathrm{B}} = (g/\bar{\rho})\,\overline{\rho w}$$

as

$$\bar{U}\frac{\partial E_{\mathrm{K}}}{\partial x} = P - F_{\mathrm{B}} - \epsilon, \tag{11}$$

$$\bar{U}\frac{\partial E_{\mathrm{P}}}{\partial x} = F_{\mathrm{B}} - 2DCN^2, \tag{12}$$

$$\bar{U}\frac{\partial P}{\partial x} = \frac{\overline{w^2}N^2}{R_i} - F_{\mathrm{B}}\frac{\partial \bar{U}}{\partial z}\frac{\overline{\rho u}}{\overline{\rho w}}, \tag{13}$$

$$\bar{U}\frac{\partial F_{\mathrm{B}}}{\partial x} = N^2(\overline{w^2} - E_{\mathrm{P}}), \tag{14}$$

where

$$N = \left(-\frac{g}{\bar{\rho}}\frac{\partial \bar{\rho}}{\partial z}\right)^{\frac{1}{2}}$$

is the Brunt-Väisälä frequency and

$$C = 3\left(\overline{\frac{\partial \rho}{\partial x}}\right)^2 \Big/ \left(\frac{\partial \bar{\rho}}{\partial z}\right)^2$$

is the Cox number.

3.2. *Exponential growth*

The approximate equation for the rate of change of turbulent kinetic energy (11) is very similar to that used by Tavoularis (1985), which successfully described the exponential downstream development of turbulent kinetic energy in the asymptotic range of a non-stratified uniform-mean shear flow. It is therefore attractive to try to extend the analysis of Tavoularis to include dynamically active stable stratification. The assumptions made by Tavoularis were: two-dimensional, steady rectilinear mean velocity $\bar{U}(z) = \bar{U} + (\partial\bar{U}/\partial z)\,z$, $(\partial\bar{U}/\partial z)$ = constant; and statistical stationarity in the laboratory frame with Reynolds stresses and pressure–velocity covariances uniform in the transverse plane (y, z). (Note, as discussed in RIHV, Tavoularis' conclusions are independent of vertical homogeneity.) Neglecting the turbulent and viscous transport terms, which experimentally have been shown (TC, HGC) to be small, the approximate turbulent-kinetic-energy equation becomes

$$\bar{U}\frac{\partial(\frac{1}{2}\overline{q^2})}{\partial x} \approx -\overline{uw}\frac{\partial\bar{U}}{\partial z} - \epsilon = P - \epsilon. \tag{15}$$

For our similar but actively stratified experimental conditions, the buoyancy flux appears on the right-hand side of (15) to give (11). Introducing $K_{12} = \overline{uw}/\overline{q^2}$, the turbulent diffusivities of momentum $K_m = \overline{uw}/(\partial\bar{U}/\partial z)$ and mass $K_z = \overline{\rho w}/(\partial\bar{\rho}/\partial z)$, and the gradient Richardson number R_i, (11) can be rewritten as:

$$\frac{\partial\overline{q^2}}{\partial x} = -K_{12}\frac{2}{\bar{U}}\frac{\partial\bar{U}}{\partial z}\left(1 - \frac{\epsilon}{P} - R_i\frac{K_z}{K_m}\right)\overline{q^2}. \tag{16}$$

If K_{12}, ϵ/P and $R_i K_z/K_m$ are independent of x or change very slowly with x, then

$$\overline{q^2} \approx \overline{q_r^2}\exp\left[-2K_{12}(\tau - \tau_r)\left(1 - \frac{\epsilon}{P} - R_i\frac{K_z}{K_m}\right)\right], \tag{17}$$

where $\tau = (x/\bar{U})(\partial\bar{U}/\partial z)$ and $\overline{q_r^2}$ is a reference value of the turbulent kinetic energy at a location $\tau = \tau_r$ within the asymptotic region. In the limit as R_i goes to zero, (17) reduces to the exponentially growing solution of Tavoularis (1985).

Whether or not K_{12}, ϵ/P and $R_i(K_z/K_m)$ have a sufficiently weak dependence on x cannot be conclusively established by the present measurements, but a strong x-dependence can be discounted. In practice R_i can be maintained nearly constant throughout the course of the experiment. K_z/K_m is known (Webster 1964) to remain constant for both passive and weakly active stratified flows. The computer simulations by Elghobashi, Gertz & Schumann (1985) for values of $R_i = 0.01$ and 0.1 found the non-dimensional cross-correlations $\overline{uw}/u'w'$ and $\overline{tw}/t'w'$ (they used temperature as their stratifying agent) to exhibit only small time variations in their asymptotic range. Finally, for $R_i < R_{i_{cr}}$ it may be reasonable to assume that ϵ/P remains nearly constant downstream, as it does for the corresponding unstratified case. It would be expected that ϵ/P should be smaller with the addition of stable stratification since now part of the energy supplied by P must be shared with $(g/\bar{\rho})\overline{\rho w}$. For the experiments presented here $[(g/\bar{\rho})\overline{\rho w}]/P$ was found to be less than 0.1.

Although (17) is only approximately correct, it offers a useful overview of the important parameters governing the development of the turbulent kinetic energy in a stratified uniform mean shear. From (17) we see that the behaviour of $\overline{q^2}$ is strongly dependent on both R_i and τ. If R_i is large enough, then $(1 - \epsilon/P - R_i(K_z/K_m))$ will be

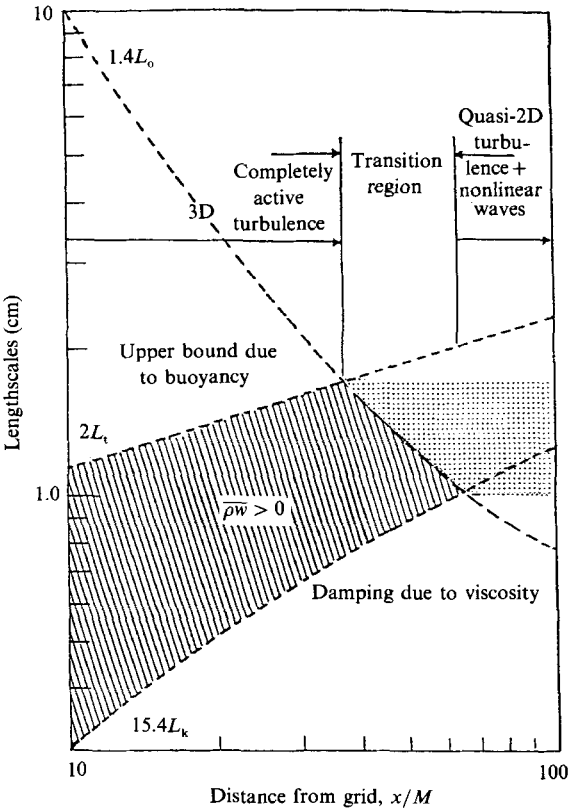

FIGURE 3. Evolution map for grid decaying stably stratified turbulence with $2L_t \ll L_0$ initially (from SHV).

negative and $\overline{q^2}$ will decay exponentially regardless of τ. Otherwise, the effect of increasing R_i is to reduce the rate at which the turbulence grows, and as $R_i \to 0$ the behaviour of the evolving turbulence approaches the unstratified case.

3.3. *Relevant lengthscales*

It is anticipated, in the present uniform-mean shear flows, that buoyancy forces may have a similar influence on the behaviour of the turbulence as they had in the previous stratified uniform-mean velocity grid-flow experiments of SHV and IHV. It is useful, then, to review the lengthscale arguments used by SHV and IHV to describe the evolution of their stratified flows.

While the size of the smallest turbulent scales are always limited by viscosity, in stably stratified decaying turbulent flows buoyancy forces also limit the size of the largest overturning scale. The measurements of SHV, for a stratified, grid-generated, decaying turbulence provide approximate limits for the range of active turbulence. The scale of motion at which buoyancy forces become of the same order of magnitude as the inertial forces is known as the Ozmidov (Dougherty 1961; Ozmidov 1965) scale:

$$L_0 = (\epsilon/N^3)^{\frac{1}{2}}. \tag{18}$$

L_0 is proportional to the upper limit permissible for the scale of turbulent motions. The smallest turbulent lengthscales are characterized by the Kolmogorov scale:

$$L_k = (\nu^3/\epsilon)^{\frac{1}{4}}, \tag{19}$$

where the viscous and inertial forces are of the same order. SHV defined the overturning scale (in a statistical sense) of their flow as being equal to $2L_t$, where

$$L_t = \frac{-\rho'}{\partial\bar{\rho}/\partial z}. \tag{20}$$

L_t was first introduced by Ellison (1957) as a typical vertical distance travelled by fluid particles before either returning towards their equilibrium level or mixing.

SHV obtained quantitative estimates for the dynamically significant relationship between the Ozmidov and Kolmogorov scales from measurements of density fluctuations and turbulent vertical mass flux. Their results suggest that active (overturning) turbulence will exist at those scales λ for which $0.7L_o > \lambda > 7.7L_k$. Figure 3 shows a schematic map of the evolution of several lengthscales in the downstream direction. The map shows the regions of the flow and the nature of the fluid motions at various stages of decay from the initial classical grid turbulence to a final state thought to consist of quasi two-dimensional turbulence and nonlinear internal waves.

4. Measurements

Conditions for the first series of measurements were identical to those of SHV (same inlet configuration, stratifications and same measuring positions) except for the addition of a uniform mean shear. To establish a baseline for comparison with the stratified-shear experiments, measurements were initially made with no density gradient and are reported in RIHV. The development of the mean-square turbulent fluctuations $(u'/\bar{U})^2$ and $(w'/\bar{U})^2$ and the shear-stress correlation coefficient $\overline{uw}/(u'w')$ essentially agreed with similar measurements of CHC at small development times τ and with TC at larger τ. The Taylor microscale was estimated using isotropic assumptions and the resulting variation with downstream position exhibited a linear growth region followed by an asymptotic approach to a constant value, also in agreement with previous measurements of CHC and TC. Finally the downstream growth of the integral lengthscale, as inferred from the one-dimensional energy spectra, was found to be consistent with that of CHC and TC. The measurements described herein were then made with a stable density stratification added to the shear. Data were predominantly taken over the central half of the test-section height where the vertical extent of the nearly constant mean velocity and density gradients remained larger than the evolving integral lengthscales.

4.1. *Evolution of turbulent velocities*

The downstream development of the non-dimensional longitudinal and vertical mean-square velocity fluctuations $(u'/\bar{U})^2$ and $(w'/\bar{U})^2$ are shown in figures 4(*a*) and 5(*a*), respectively, for different stabilities R_i. For these experiments the inlet of SHV and IHV was in place. At small x/M the turbulence is grid dominated regardless of the imposed shear or stratification, and the turbulent kinetic energy is observed to decay. However, at large x/M the shear and buoyancy forces determine the characteristics of the turbulence. The growth rates of $(u'/\bar{U})^2$ and $(w'/\bar{U})^2$ with stratification can be dramatically less than the corresponding unstratified-flow growth rates, and for large enough stabilities (R_i), the turbulent intensities are observed to decay. As the stability of the flow decreases, the growth rates approach the passive-scalar case and the limiting behaviour of the non-dimensional correlation

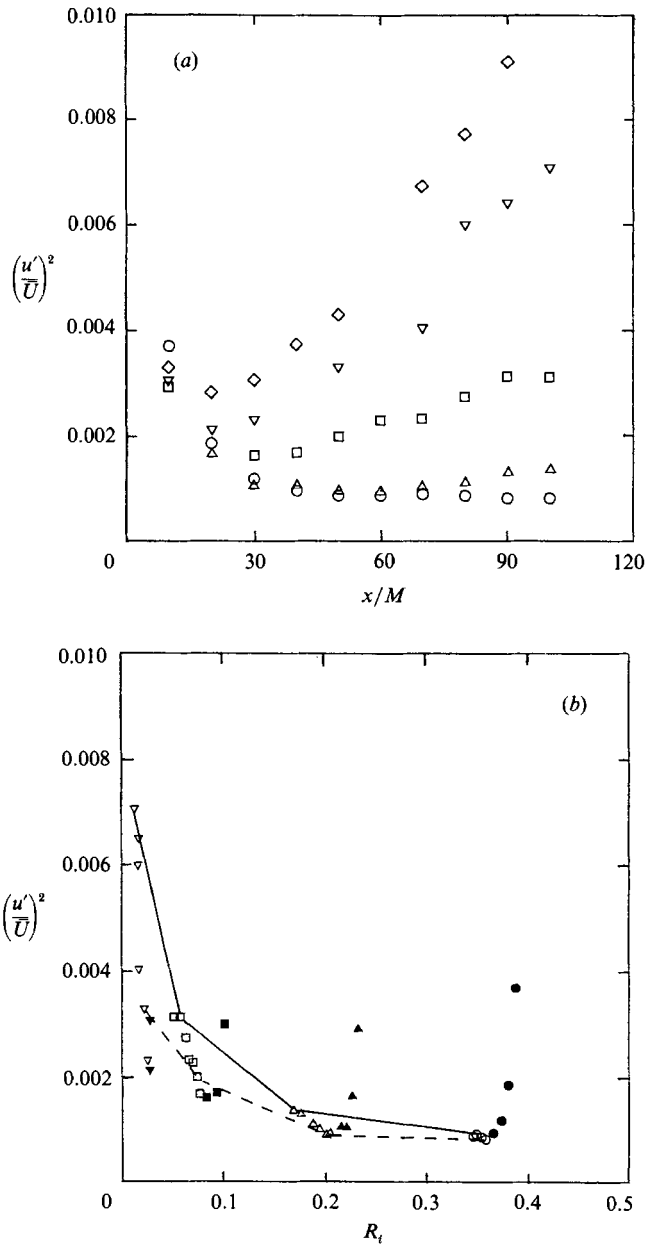

FIGURE 4. (*a*) Downstream development of streamwise turbulent kinetic energy with x/M (M = 1.905 cm). ○, $R_i \approx 0.36$; △, $R_i \approx 0.18$; □, $R_i \approx 0.06$; ▽, $R_i \approx 0.02$; ◇, $R_i = 0$. (*b*) Dependence of streamwise turbulent kinetic energy on stability R_i. Symbols as defined in (*a*). Solid symbols were taken close to the inlet and are consequently influenced by the decaying grid turbulence produced there. ——, $\tau \approx 10.1$; – – –, $\tau \approx 5.3$.

coefficients $\overline{uw}/u'w'$, $\overline{\rho w}/\rho' w'$ and $\overline{\rho u}/\rho' u'$ is found to be consistent with the passive-scalar measurements of TC.

The normalized turbulent kinetic energies $(w'/\bar{U})^2$ and $(u'/\bar{U})^2$ of figures 4(*a*) and 5(*a*) are plotted *vs.* the local gradient Richardson number R_i in figures 4(*b*) and 5(*b*), respectively. Measurements close to the inlet (included in figure 4(*a*) for comparison)

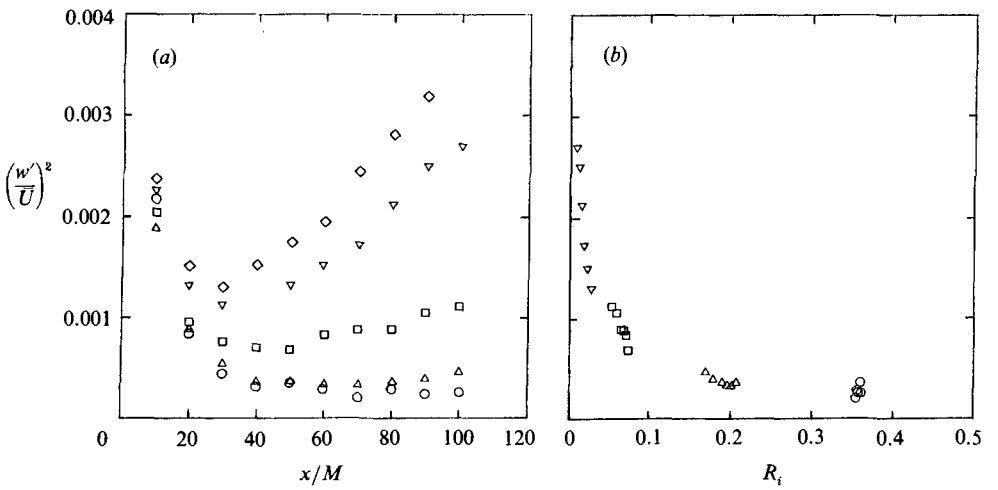

FIGURE 5. Dependence of vertical turbulent kinetic energy on x/M ($M = 1.905$ cm) in (a) and stability R_i in (b). In (b) measurements influenced by the inlet have been omitted. ○, $R_i \approx 0.36$; △, $R_i \approx 0.18$; □, $R_i \approx 0.06$; ▽, $R_i \approx 0.02$; ◇, $R_i = 0$.

are contaminated by the decaying turbulence associated with it. Initially the production term $P = -\overline{uw}/(\partial\bar{U}/\partial z)$ is very small because near the inlet the velocity fluctuations are uncorrelated ($\overline{uw} \sim 0$), and small x corresponds to small development time τ. A certain amount of flow development time ($\tau > 4$, see RIHV) is required before the interaction between the mean shear and turbulence dominates the flow. Indiscriminate comparison of data taken at small τ (upstream of the shear-dominated region) with data taken at large τ (in the shear-dominated region) may thus have led to the difficulties in interpreting Webster's earlier work (1964) as discussed in §1. However, Webster's measurements of $(w'/\bar{U})^2$ *vs.* R_i ($0.05 < R_i < 0.3$) in the region uninfluenced by the inlet are similar to those illustrated in figure 5(b). Although Webster (1964) could not obtain reliable data at smaller R_i because of background temperature fluctuations, he anticipated the $(w'/\bar{U})^2$ dependence on small R_i found in figure 5(b). No $(u'/\bar{U})^2$ *vs.* R_i measurements were reported by Webster to compare with the corresponding values of figure 4(b).

The gradient Richardson number for the largest stratifications (in figures 4–7) varied monotonically between 0.39 and 0.36 with increasing x/M, and nowhere was the turbulent energy observed to grow. The remaining stratifications all produced gradient Richardson numbers less than 0.21, and downstream of the region influenced by the grid the turbulent intensities grow at a rate that increases with decreasing stratification. The Miles (1961) criterion for stability of an inviscid, laminar, continuously stratified flow to infinitesimal disturbances requires a gradient Richardson number greater than 0.25. Although this value is consistent with the present data, the Miles criterion cannot be strictly applied since the grid at the inlet creates finite disturbances (i.e. turbulent flow) not amenable to a linear stability analysis. For nonlinear stability (Abarbanel *et al.* 1984) of parallel laminar shear flow in a three-dimensional stratified fluid the necessary and sufficient condition for formal stability everywhere in the flow is

$$N_{R_i}(z) = N(z)^2 \Big/ \left[\left(\frac{\partial\bar{\rho}}{\partial z}\right)^2 \frac{\partial^2}{\partial\bar{\rho}^2}[\tfrac{1}{2}\bar{U}^2(z)]\right] > 1. \tag{21}$$

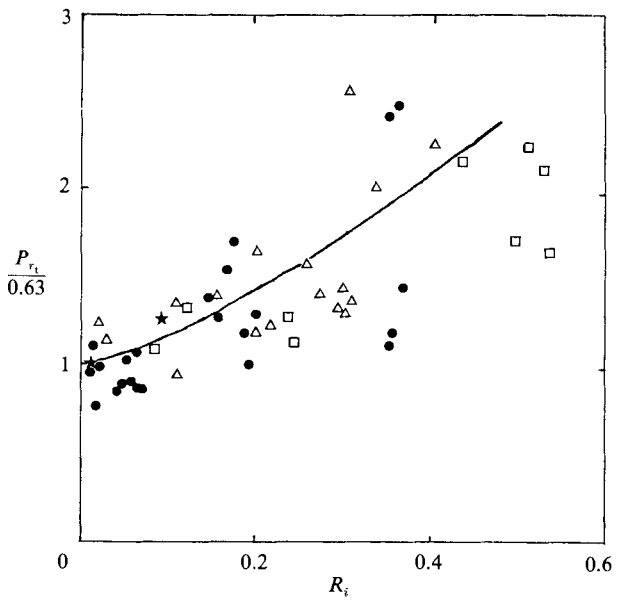

FIGURE 6. Normalized turbulent Prandtl number (P_{r_t}) as a function of R_i. ——, Launder's (1975) predictions; ★, Elghobashi *et al*'s (1985) numerical calculations; △, □, Webster's (1964) measurements at two stations; ●, present data.

For the present laboratory flows in which the turbulence develops in density and velocity fields with nearly constant gradients, $N_{R_i}(z) = R_i$.

If the non-dimensional quantities $-\overline{uw}/q^2$, ϵ/P and K_z/K_m (which are always positive) approach nearly constant values as the turbulence grows downstream, independent of R_i (for $R_i < R_{i_{cr}}$), then $R_{i_{cr}}$ can be estimated from (17) by setting $1-\epsilon/P-R_i(K_z/K_m) = 0$. Smaller values of R_i will guarantee a positive exponent and consequently an increase in $\overline{q^2}$ with increasing τ. Unfortunately neither $-\overline{uw}/q^2$, ϵ/P nor K_z/K_m have been adequately determined, and furthermore they probably depend on R_i, although this dependence may be weak for small R_i (i.e. $R_i < R_{i_{cr}}$). The values of $-\overline{uw}/q^2$ and ϵ/P for growing turbulent shear flows without active stratification are 0.155 ± 0.015 and 0.645 ± 0.075 respectively (see Karnik & Tavoularis 1983). For both weakly active ($R_i < 0.01$) and passively stratified shear flows K_z/K_m is found to be around 1.35 (Webster 1964). In figure 6 the turbulent Prandtl number ($P_{r_t} = [K_z/K_m]^{-1}$), normalized by its value for non-stratified flows $P_{r_0} = 0.63$, is plotted as a function of R_i for both Webster's and the present data. Also included are the modelling predictions by Launder (1975) and the numerical simulations of Elghobashi *et al.* (1985). The measurements in figure 6 suggest that for $R_i < R_{i_{cr}}$, P_{r_t} may not be strongly dependent on R_i. The large spread in the experimental data results from the uncertainty in measuring $\overline{uw}$ and $\overline{\rho w}$. The following values are a representative average (individual values may differ by as much as 50% between experiments) of the present data obtained far from the inlet:

$$-\frac{\overline{uw}}{q^2} \approx 0.16, \quad \frac{\epsilon}{P} \approx 0.6, \quad \frac{K_z}{K_m} \approx 1.4.$$

Together with (17) these values estimate $R_{i_{cr}}$ to be about 0.29, reasonably close to the experimental estimate of $R_{i_{cr}} = 0.25\pm0.05$.

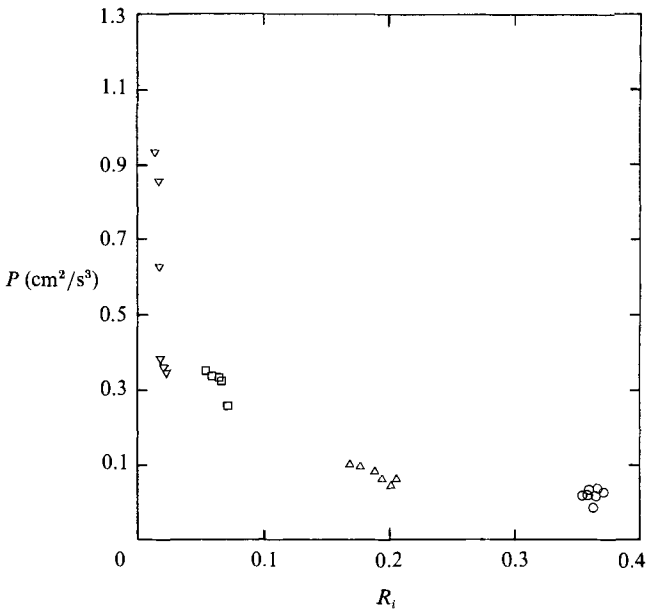

FIGURE 7. Dependence of turbulent kinetic-energy production ($P = -\overline{uw}(\partial\bar{U}/\partial z)$) on stability R_i. Symbols as defined in figure 4(*a*). For each symbol, higher values of P correspond to larger development times τ.

In figure 7 the production term, $P = -\overline{uw}(\partial\bar{U}/\partial z)$, is plotted as a function of R_i. Only measurements for x/M beyond the influence of the inlet are included. Even with the relatively greater variance in measuring $\overline{uw}$, the overall dependence of P on R_i is clear. The decrease of the correlation between the longitudinal and vertical velocity fluctuations with increasing R_i is the principal reason for the decrease in the growth rate of turbulent kinetic energy with increasing R_i. As shown by SHV, stable stratifications primarily suppress the larger overturning scales of the turbulence. It is these scales that make the biggest contribution to $\overline{uw}$.

Excluding those measurements dominated by the turbulence produced by the inlet, the question remains as to whether the turbulent kinetic energy is determined by R_i alone. It has been argued in §3.2 that developing turbulence in a stratified, uniform mean shear should depend strongly on both R_i and τ. When $(u'/\bar{U})^2$, $(w'/\bar{U})^2$, and $-\overline{uw}(\partial\bar{U}/\partial z)$ are plotted *vs.* R_i (figures 4*b*, 5*b* and 7), they show a clear overall decrease with increasing R_i. When in figure 4(*b*) the corresponding τ-values are indicated some τ-dependence is also evident when $R_i < R_{i_{cr}}$. It is found, as predicted by (17), that for a fixed evolution time τ the longitudinal kinetic energy decreases with R_i, while for nearly constant R_i, u'^2/U^2 increases with larger τ. Similar results were found for the vertical kinetic energy.

To ascertain whether the behaviour observed in figures 4–7 persists for longer flow development times it was necessary to rebuild and modify the water-channel inlet such that a uniform mean shear could be successfully maintained significantly further downstream. Achieving this also resulted in reducing the rate of decay of the density profile. The effective length over which useful measurements could be taken was more than doubled, corresponding to maximum development times of $\tau \approx 25$. The $(w'/\bar{U})^2$ measurements are shown in figure 8(*a*). Clearly, the dependence on x/M exhibited in figure 5(*a*) is preserved further downstream. For the case in

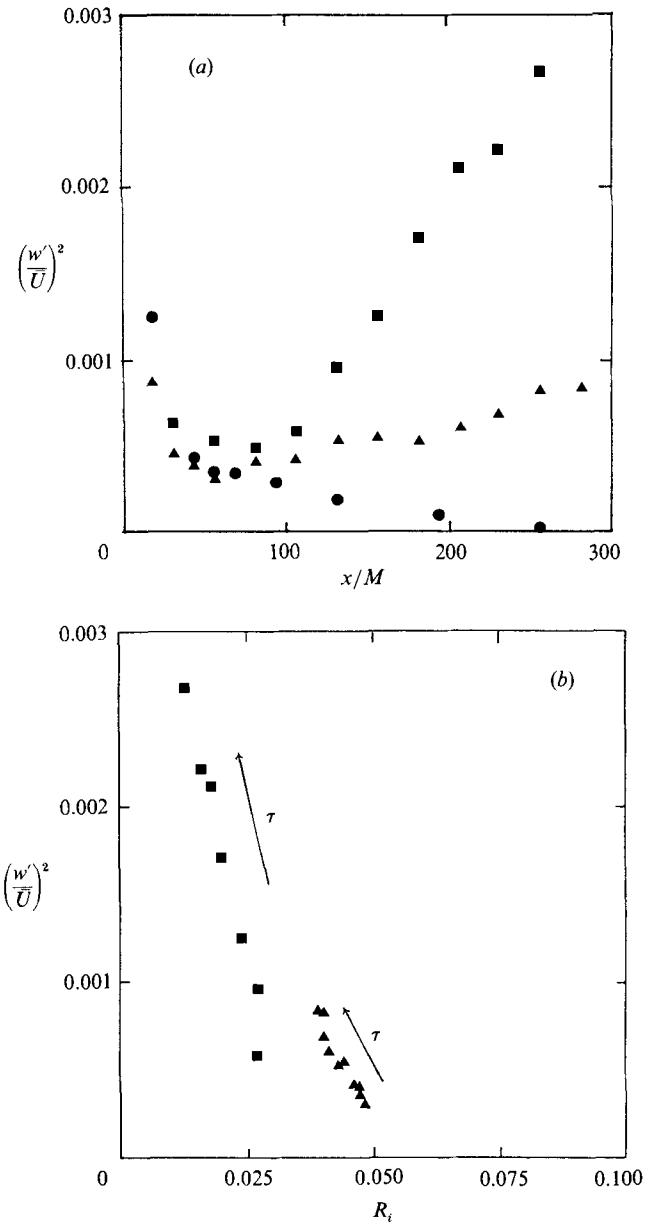

FIGURE 8. Downstream development (with diffuser) of vertical turbulent kinetic energy with (*a*) x/M ($M = 1.524$ cm) and (*b*) R_i. ●, R_i ($\sim 0.26 \pm 0.03$) $\geqslant R_{i_{cr}}$; ▲, $R_i \approx 0.04$; ■, $R_i \approx 0.02$. For each symbol, higher values of $(w'/\bar{U})^2$ correspond to larger development times τ.

figure 8(*a*) for which $(w'/\bar{U})^2$ is observed to monotonically decay, R_i is estimated to be about 0.26. It should be noted that because the velocity profile, in this particular instance, developed a kink midway in its height (at the measuring position), there was a 15% uncertainty associated with estimating R_i.

Plotting the same values of $(w'/\bar{U})^2$ from figure 8(*a*) *vs.* R_i in figure 8(*b*), it becomes apparent that τ can be as important a parameter as R_i in determining the growth of

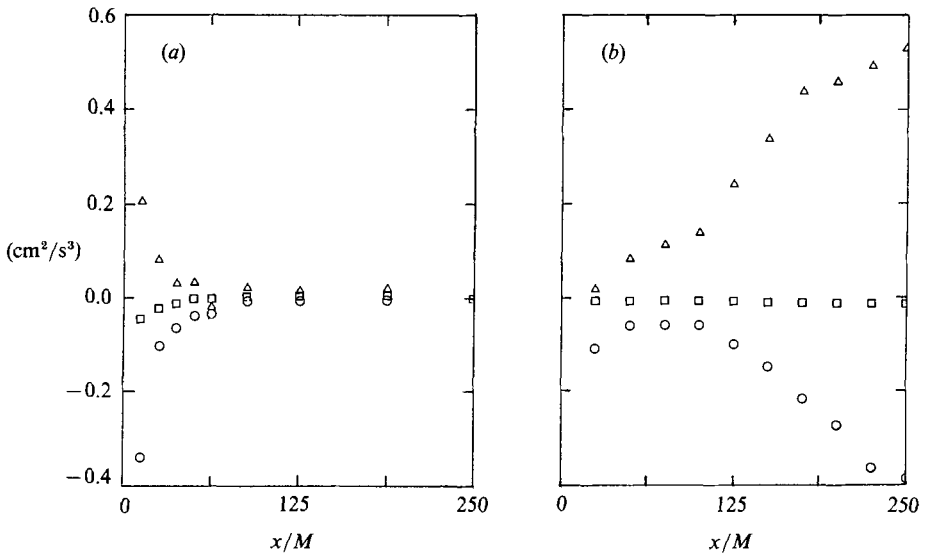

FIGURE 9. Downstream development of the principal terms acting as sources and sinks in the turbulent kinetic energy equation. (*a*) $R_i \approx 0.26 \pm 0.04 > R_{i_{cr}}$; (*b*) $R_i = 0.02 < R_{i_{cr}}$; △, $-\overline{uw}(\partial\bar{U}/\partial z)$; □, $(-g/\bar{\rho})\overline{\rho w}$; ○, $-\epsilon$.

the turbulent kinetic energy. Similar behaviour is observed for both $(u'/\bar{U})^2$ and $-\overline{uw}(\partial\bar{U}/\partial z)$.

Figures 9(*a*) and 9(*b*) contrast, for decaying and growing turbulence in stratified shear flows, the downstream development of the principal terms acting as sources and sinks of turbulent kinetic energy (equation (11)). The buoyancy flux $(g/\bar{\rho})\overline{\rho w}$ is observed to act only as a weak sink even when $R_i < R_{i_{cr}}$. The dissipation (ϵ)† always decreases immediately behind the grid, but for $R_i < R_{i_{cr}}$ it grows (note that for clarity $-\epsilon$ is plotted in figure 9) further downstream with the increasing turbulence intensity. The production term $-\overline{uw}(\partial\bar{U}/\partial z)$ is observed to respond strongly to the presence of the mean shear only when $R_i < R_{i_{cr}}$.

4.2. *Evolution of lengthscales*

The present experiments can be used to determine whether the SHV and IHV lengthscale analysis is applicable to stably stratified, uniform-mean shear flows. When $R_i > R_{i_{cr}}$, the coefficients of L_0 and L_k which delineate the range of overturning lengthscales (see §3.3) can be determined using the same procedures as SHV. This is accomplished by measuring the ratio L_t/L_0 at the point where the growth of L_t first deviates from the curve describing a passive growth (Montgomery 1974), and measuring the ratio L_0/L_k at the estimated point where $\overline{\rho w}$ first goes to zero. These transition points are found to exist only when $R_i > R_{i_{cr}}$, i.e. when the turbulence

† The isotropic relation $\epsilon = \nu[10\overline{(\partial u/\partial x)^2} + 2.5\overline{(\partial w/\partial x)^2}]$ has been used, where $\overline{(\partial u/\partial x)^2}$ and $\overline{(\partial w/\partial x)^2}$ are calculated by integrating k^2 times the one-dimensional energy spectra of $E_{uu}(k)$ and $E_{ww}(k)$, respectively. TC had found for uniform mean shear flows that $\epsilon \approx 8.5\nu\overline{(q^2/u'^2)}\overline{(\partial u/\partial x)^2}$ or since $\overline{q^2} \approx 1.89\overline{u'^2}$, $\epsilon \approx 16.07\nu\overline{(\partial u/\partial x)^2}$. They also found that $\overline{(\partial w/\partial x)^2} \approx 2.6\overline{(\partial u/\partial x)^2}$ so that the isotropic relation for the dissipation can be rewritten as $\epsilon \approx 16.5\nu\overline{(\partial u/\partial x)^2}$, which is close to TC's estimate for the uniform-mean-shear case.

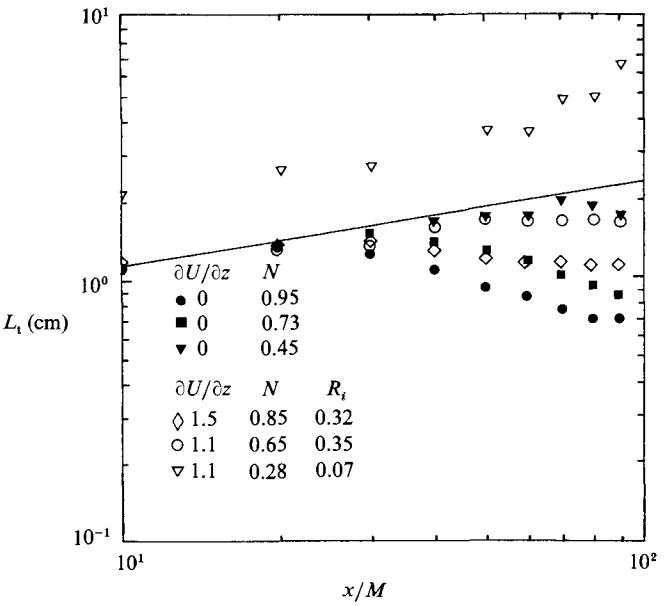

FIGURE 10. Dependence of the overturning turbulent lengthscale on x/M (M = 1.905 cm). Solid symbols = L_t of SHV, $\partial U/\partial z = 0$. Open symbols = L_t of present data. Solid line = passive temperature scalar growth ($L_t = (T'/(\partial\bar{T}/\partial z))$ found by Montgomery (1974), $\partial U/\partial z = 0$.

decays. When $R_i < R_{i_{cr}}$, L_t is observed to continually grow and $\overline{\rho w}$ never decreases to zero (disregarding the trivial case where $\partial\bar{\rho}/\partial z$ goes to zero).

For the two decaying-shear cases studied (with the same inlet grid as SHV and IHV), it is found that the range of overturning scales is approximately $1.1L_o > \lambda > 8.8L_k$, very close to the similarly stratified but unsheared measurements of SHV and IHV. In figure 10 the behaviour of L_t for $R_i < R_{i_{cr}}$ is contrasted with that for $R_i > R_{i_{cr}}$. Also included in figure 10 for comparison are Montgomery's† and SHV's measurements. The remarkable similarity between the shear data when $R_i > R_{i_{cr}}$ and the SHV data suggests that when $R_i > R_{i_{cr}}$ the shear may only marginally influence the development of L_t.

For the decaying turbulence ($R_i > R_{i_{cr}}$), uniform-mean shear-flow data it is found that, when $L_o \approx 8L_k$, all overturning scales have been effectively suppressed ($\overline{\rho w} = 0$) owing to the combined effect of buoyancy and viscosity. By substituting the definitions of L_o and L_k into $L_o = 8L_k$ the transition dissipation rate ϵ_{tr} is calculated to be equal to $16\nu N^2$, close to the unsheared case value of $15\nu N^2$ (IHV, 1986). In the region beyond the influence of the grid, it is observed that for $R_i > 0.3$, $\epsilon < \epsilon_{tr}$ and the turbulence decays, while for $R_i < 0.2$, $\epsilon > \epsilon_{tr}$ and the turbulence grows. Therefore, the simple ϵ-criterion for the existence of turbulence is applicable both to sheared and unsheared decaying turbulence. Figure 11 plots ϵ *vs.* νN^2 for the present data as well as the SHV data. As shown for either data set, the boundary $\epsilon = 16\nu N^2$ serves well in separating the overturning and non-overturning domains. For smaller R_i, as the shear becomes a more effective source for turbulence, ϵ can grow much larger than ϵ_{tr}.

SHV found that for grid-generated, decaying, stably stratified turbulence, if the

† Montgomery's data was normalized by the ratio of his grid mesh size to that used in the water channel since the mesh size induces an initial lengthscale to the turbulence.

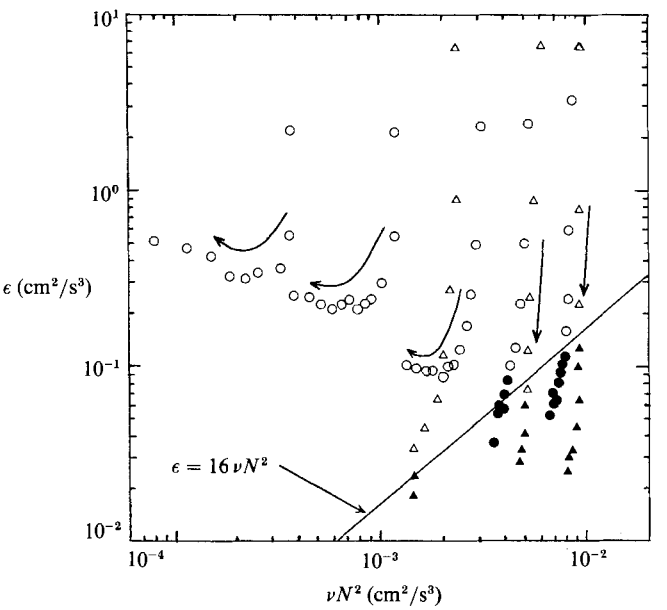

FIGURE 11. Transition boundary between turbulent and non-turbulent domains. ——, $\epsilon_{tr} = 16\nu N^2$; △, SHV unsheared data, $\overline{\rho w} > 0$; ▲, SHV unsheared data, $\overline{\rho w} \sim 0$; ○, present sheared data, $\overline{\rho w} > 0$; ●, present sheared data, $\overline{\rho w} \sim 0$. The arrows indicate increasing distance from the grid.

density gradient is strong enough, the turbulence is suppressed so quickly that incomplete scalar mixing occurs. This results in restratification as evidenced by a negative buoyancy flux ($(g/\bar{\rho})\overline{\rho w}$). Since the initial separation distance between the turbulent (L_t) and buoyancy limiting (L_o) lengthscales is related (in decaying turbulence) to the persistence time of the turbulence, a restratification criterion can be based on the initial ratio L_t/L_o. From their measurements, SHV estimated initial values of $L_t/L_o \leqslant 0.15$, as their upper bound for the criterion for complete mixing (where the lengthscales were measured at $x/M = 10$). With the addition of a uniform mean shear it is found that, if $R_i < R_{i_{cr}}$ restratification is never observed. However, for the case $R_i > R_{i_{cr}}$ the SHV criterion is still found to work reasonably well. Komori *et al.* (1983) also found restratification occurring (their figure 7) for local gradient Richardson numbers near 0.25 and greater in their stably (temperature) stratified shear flows.

In a mixing layer composed of two parallel streams of water having different densities, Koop & Browand (1979) have studied the major features of the turbulence produced. They found (for global Richardson numbers $R_{i_0} < 0.15$) that a stably stratified density difference, no matter how small, acts ultimately to collapse and relaminarize the turbulence. Preceding this downstream location where restratification begins, Koop & Browand (1979) observed a turbulent growth region characterized by large quasi-organized vortical structures, familiar to unstratified-mixing-layer studies. Although in many ways mixing layers and the present uniform mean shear flow are inherently different, e.g. global Richardson numbers and gradient Richardson numbers cannot be unambiguously compared, we found some general similarities worth mentioning. In both flows, providing that the mean shear can sustain growing turbulent lengthscales, no restratification is observed. Because for the present measurements the turbulent lengthscale L_t remains sufficiently

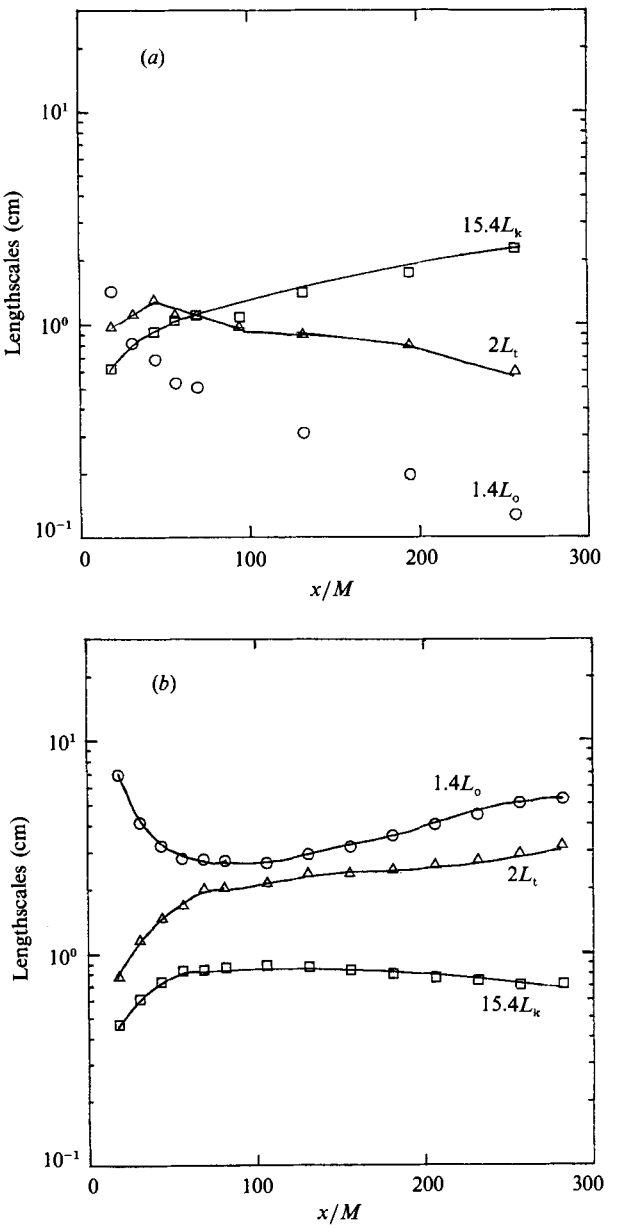

FIGURE 12(*a*,*b*). For caption see facing page.

smaller than the extent of the linear mean velocity profile, if L_t begins to grow ($R_i < R_{i_{cr}}$) it will continue to. When $R_i > R_{i_{cr}}$, however, the flow stability is too great for the mean shear to initiate the growth of L_t. Koop & Browand (1979) also notice that at larger stabilities ($R_{i_0} > 0.15$) a different sequence occurs, the flow is no longer characterized by large vortices but by interfacial waves. Although the prevalence of internal waves in the present facility has been found (IHV) to depend in part on the inlet configuration, for the stratified uniform mean shear flows investigated, only if $R_i > R_{i_{cr}}$ were internal waves clearly observed in the vertical turbulent velocity spectra (Rohr 1985).

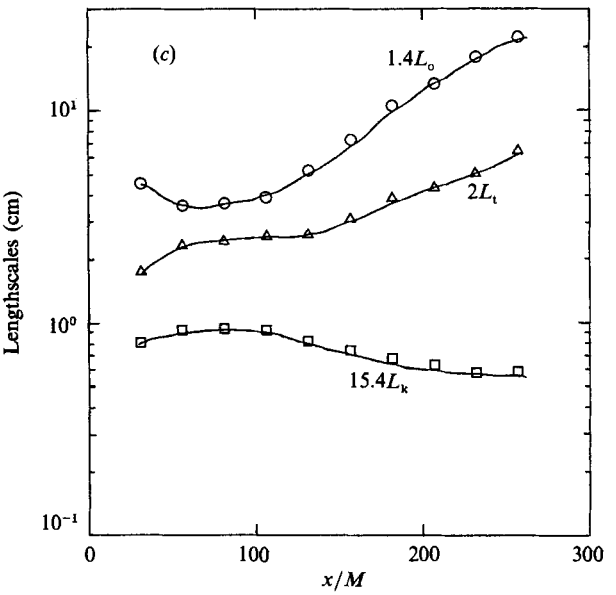

FIGURE 12. Evolution map for growing turbulence in a stably stratified uniform mean shear with $L_t \ll L_o$ initially and (*a*) $R_i \sim 0.26 \geqslant R_{i_{cr}}$; (*b*) $R_i \sim 0.04 \leqslant R_{i_{cr}}$; (*c*) $R_i \sim 0.02 \ll R_{i_{cr}}$. ○ = $1.4(\epsilon/N^3)^{\frac{1}{2}}$; △ = $2\rho'/(\partial\bar{\rho}/\partial z)$; □ = $15.4(\nu^3/\epsilon)^{\frac{1}{4}}$.

In figure 12(*a*) an SHV lengthscale evolution 'map' is drawn for the case $R_i > R_{i_{cr}}$. This 'map' extends much farther downstream ($x/M = 260$ compared with 100 for SHV – see figure 3), but the underlying features are the same. For $R_i < R_{i_{cr}}$ the previous lengthscale 'map' of SHV changes dramatically. In figure 12(*b*) for $R_i = 0.04$ it is observed that beyond the immediate influence of the grid ($x/M > 60$) both L_t and L_o grow, with L_o growing the fastest. Thus, for the case of shear-generated growing stratified turbulence, the growth rate of L_o appears to determine the growth rate of the turbulent scale L_t as it did in the stratified uniform mean flows of SHV and IHV. In the same region of the flow L_k decreases since ϵ increases with the growing turbulence. Therefore, the range of overturning scales increases downstream. As shown in figure 12(*c*), reducing the stability further ($R_i = 0.02$) results in increasing both the rates of growth of L_o and L_t and the separation between L_o, $L_t$and L_k.

In a stably stratified flow, as the overturning scale increases so must the influence of stabilizing buoyancy forces. Without some compensating input benefiting inertial forces, the growth of the vertical scales must eventually be limited. This is evidenced in the vertical growth limitations of wakes (Lin & Pao 1979), mixing layers (Koop & Browand 1979) and intrusions (Ivey & Corcos 1982) in stably stratified flows. However, the effect of stable stratification in a uniform mean shear flow when $R_i < R_{i_{cr}}$ does not limit the absolute size of the largest overturning lengthscale. Instead its effect is to reduce the growth rate of the turbulent lengthscales (L_t and L_o) from their unstratified rates of growth. The downstream growth of L_t is not arrested by the increasing influence of stabilizing buoyancy forces because the favourable interaction between the overturning scales and the mean shear also increases with L_t. As previously mentioned, when $R_i \geqslant R_{i_{cr}}$ the lengthscales do not continue to grow but evolve similarly to the results of SHV for their corresponding unsheared case.

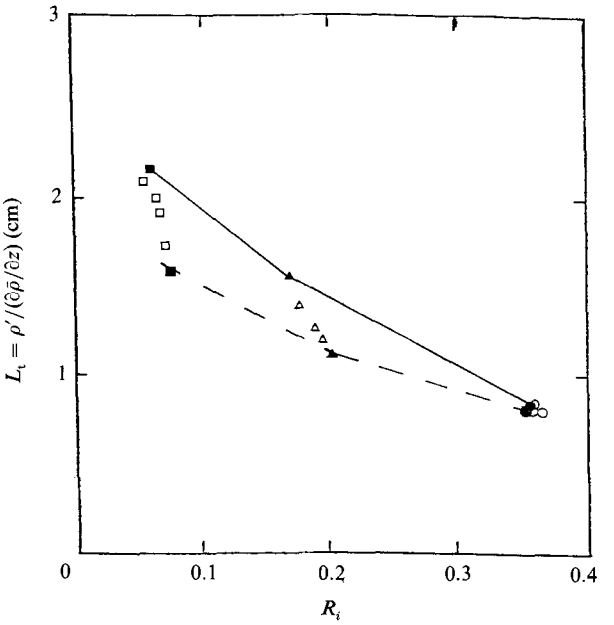

FIGURE 13. Dependence of L_t on R_i. Symbols same as in figure 4. ——, $\tau \approx 10.1$; – – –, $\tau \approx 5.3$.

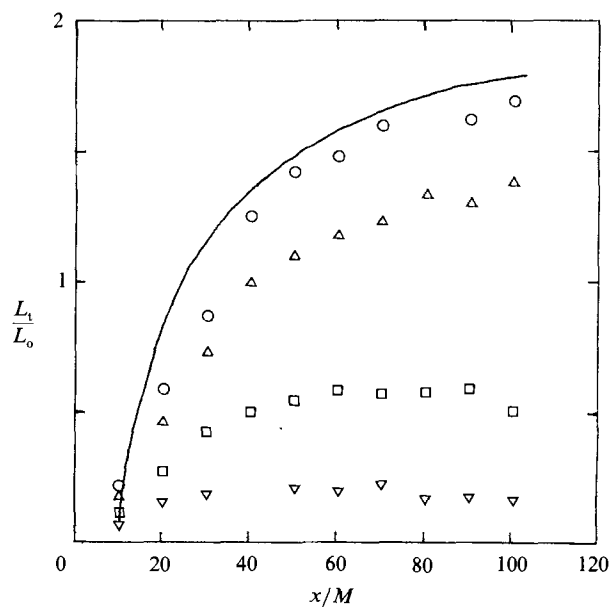

FIGURE 14. Downstream development of the ratio of observed overturning (L_t) to buoyancy limiting (L_o) scales. ——, L_t of SHV for $N = 0.96$. Symbols same as in figure 4.

Figure 13 shows some of the accompanying values of L_t and R_i for the data of figure 4(*a*) at measuring positions beyond the influence of the inlet. As in figures 4(*b*) and 8(*b*) for the turbulent intensities, L_t shows a strong dependence on τ. At constant τ, L_t exhibits a dependence on R_i similar to that found by Webster (1964, figure 15) for his measurements uninfluenced by the inlet. For Webster's measurements τ was approximately constant because, at a fixed position, τ can only vary with

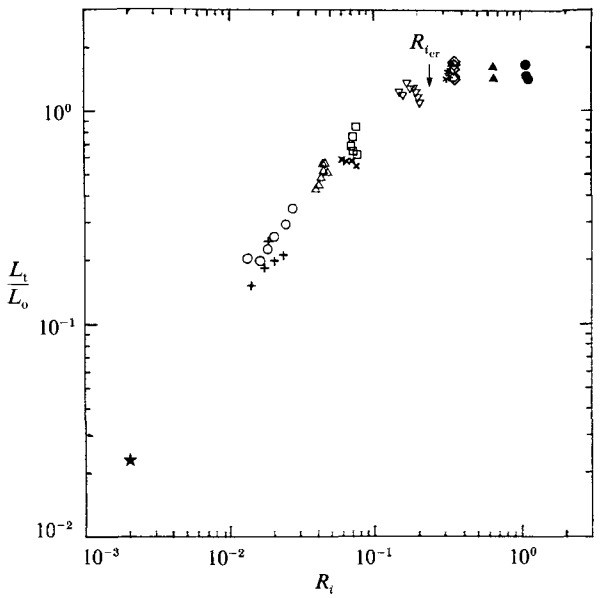

FIGURE 15. The ratio of observed overturning (L_t) to buoyancy limiting (L_o) scales *vs.* stability (R_i). ▲, ● from Stillinger (1981); ★ from Tavoularis & Corrsin (1981); remaining symbols from present data. Point where $R_i \approx R_{i_{cr}}$ is shown by arrow.

$(1/\bar{U})(\partial\bar{U}/\partial z)$. The shear-generating grid of Owen & Zienkiewicz (1957) used by Webster produces only constant values of $(1/\bar{U})(\partial\bar{U}/\partial z)$. The mean shear and centreline velocity can be varied independently by using either a shear generator consisting of separate channels, each filled with a series of interchangeable screens to produce the necessary pressure drop (Karnik & Tavoularis 1987), or as in the present experiments, simply driving each layer separately.

In SHV's experiment the overturning scale L_t, owing to buoyancy effects, eventually 'locks in' on the decaying buoyancy scale L_o and remains nearly proportional to it. With the addition of a uniform mean shear it is found that the ratio of L_t/L_o is strongly dependent on R_i. This is illustrated in figure 14, where the corresponding values of L_t/L_o for measurements taken with the same SHV inlet (figures 4–7) are plotted *vs.* x/M. It is seen that L_t/L_o increases with increasing flow stability, until $R_i > R_{i_{cr}}$, where it approaches the value of SHV's unsheared measurements.

The downstream behaviour of L_t/L_o for both decaying (Rohr, Itsweire & Van Atta 1984) and growing (Rohr & Van Atta 1987) turbulent flows has been found to be related to the mixing efficiency of the flow. It has been found that if the largest lengthscale of the flow is still overturning (as is guaranteed if $R_i < R_{i_{cr}}$) then both the mixing efficiency and L_t/L_o grow with stability R_i. This result is in agreement with the experimental evidence that collapsing Kelvin–Helmholtz instabilities and breaking internal waves produce the highest observed mixing efficiencies (Linden 1979). Figure 15 shows a compilation of L_t/L_o in the shear-dominated region as a function of R_i for all the present stably stratified-shear experiments. Also included are the higher-R_i experiments of Stillinger (1981) as well as the extremely low-R_i (passively stratified) experiments of TC. The degree of collapse of all the data to a single curve is extraordinarily good. The break in the L_t/L_o *vs.* R_i curve

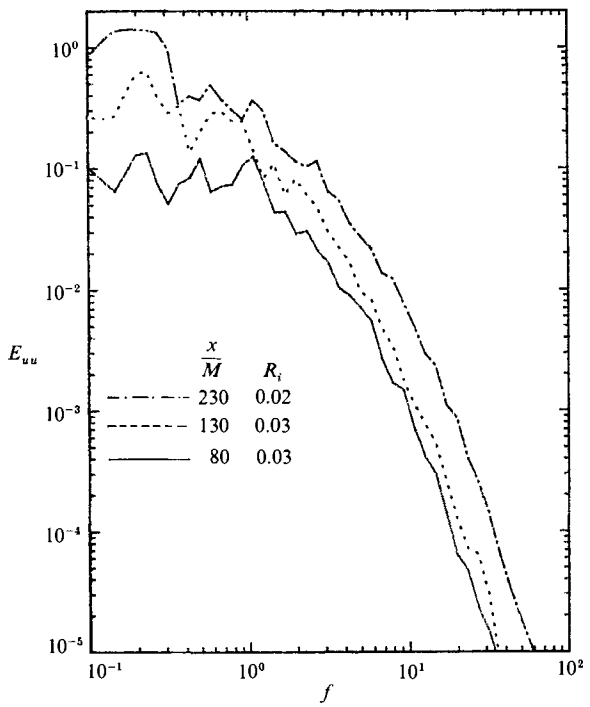

FIGURE 16. Downstream development of one-dimensional spectra of the streamwise turbulent velocity, $0 < R_i < R_{i_{cr}}$.

at $R_{i_{cr}}$ (≈ 0.25) is consistent with the observation (figures 4*a* and 5*a*) that near $R_i \approx 0.25$ there is an abrupt change in the turbulence evolution i.e. for $R_i \leqslant 0.25$ the turbulence grows while for $R_i \geqslant 0.25$ the turbulence decays.

5. Spectral measurements

Figures 16–19 show the effects of different stable stratifications on the evolving one-dimensional energy spectra. When the gradient Richardson number R_i is less than the critical value $R_{i_{cr}}$, turbulent fluctuations are observed to increase downstream. The associated $E_{uu}(f)$ spectral evolution for large flow development times τ is illustrated in figure 16 for values of x/M equal to 80, 130 and 230 (or τ of 7.4, 11.8 and 18.0 respectively). Except for their slower evolution owing to the effects of stratification, these developing spectral shapes resemble those of the unstratified shear case (RIHV). The effects of stratification can be better observed in figure 17 where the $E_{uu}(f)$ spectra are plotted for different stabilities at nearly the same value of τ. The collapse of these spectra is good when non-dimensionalized by the respective Kolmogorov length and velocity scales, as shown in figure 18. Comparing the dimensional and Kolmogorov normalized spectra of the unstratified shear flows (RIHV, their figures 13–16) with the stratified shear flows (figures 17 and 18*a*; $R_i < R_{i_{cr}}$), it appears that the development of the spectra is much the same with either increasing τ (RIHV) or decreasing stratification.

The data represented by the solid circles in figure 18(*a*) were derived from TC's uniform shear spectrum. These data were taken at $x/H = 10.5$ and normalized by the appropriate ϵ- and ν-values listed in table 4 of TC. TC's measurements were taken in

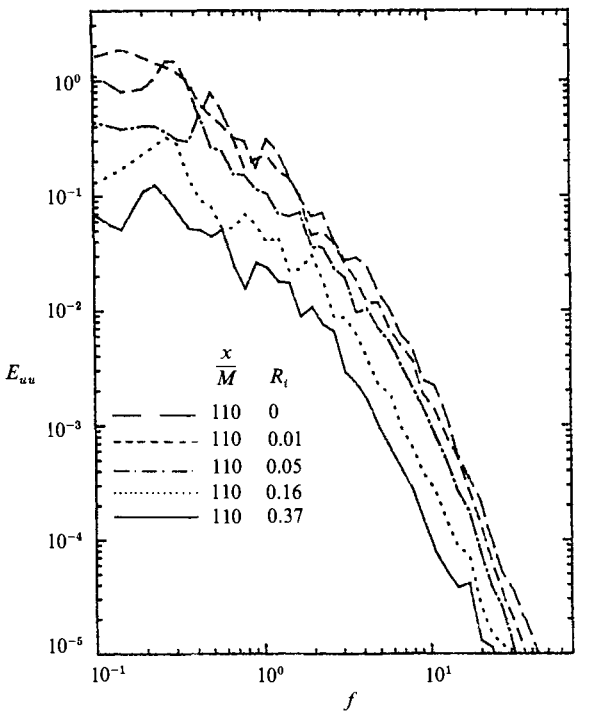

FIGURE 17. One-dimensional spectra of the streamwise turbulent velocity for nearly constant τ (~ 10) and varying R_f.

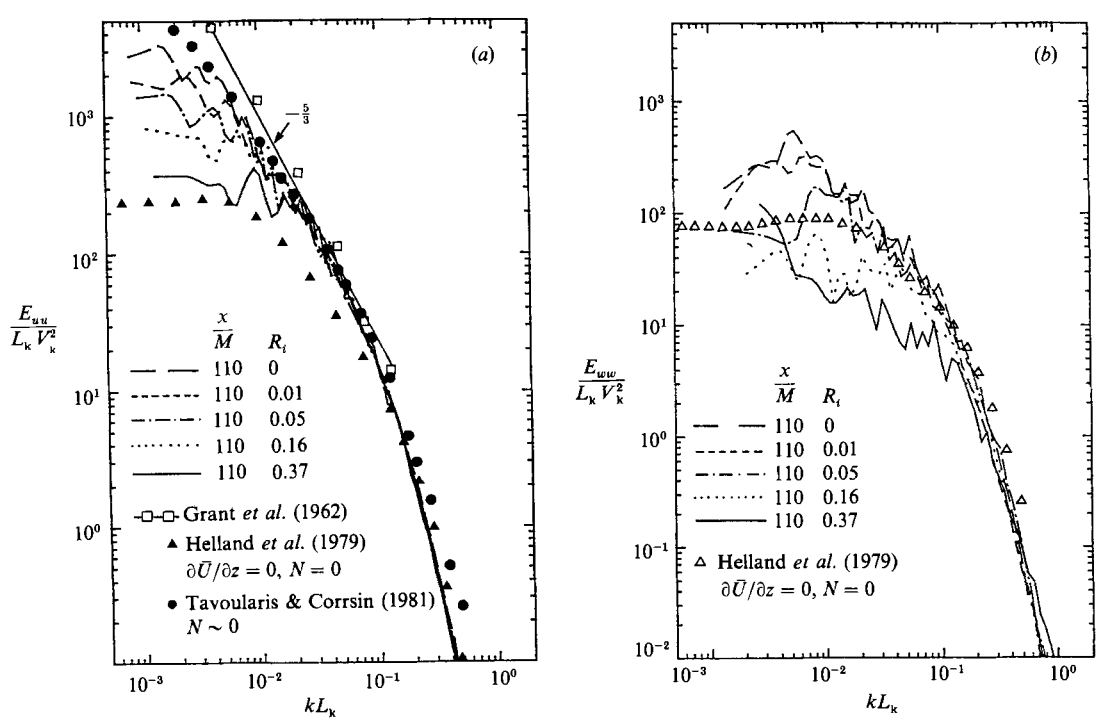

FIGURE 18. (*a*) Normalized one-dimensional turbulent streamwise velocity spectra. (*b*) Normalized one-dimensional turbulent vertical velocity spectra.

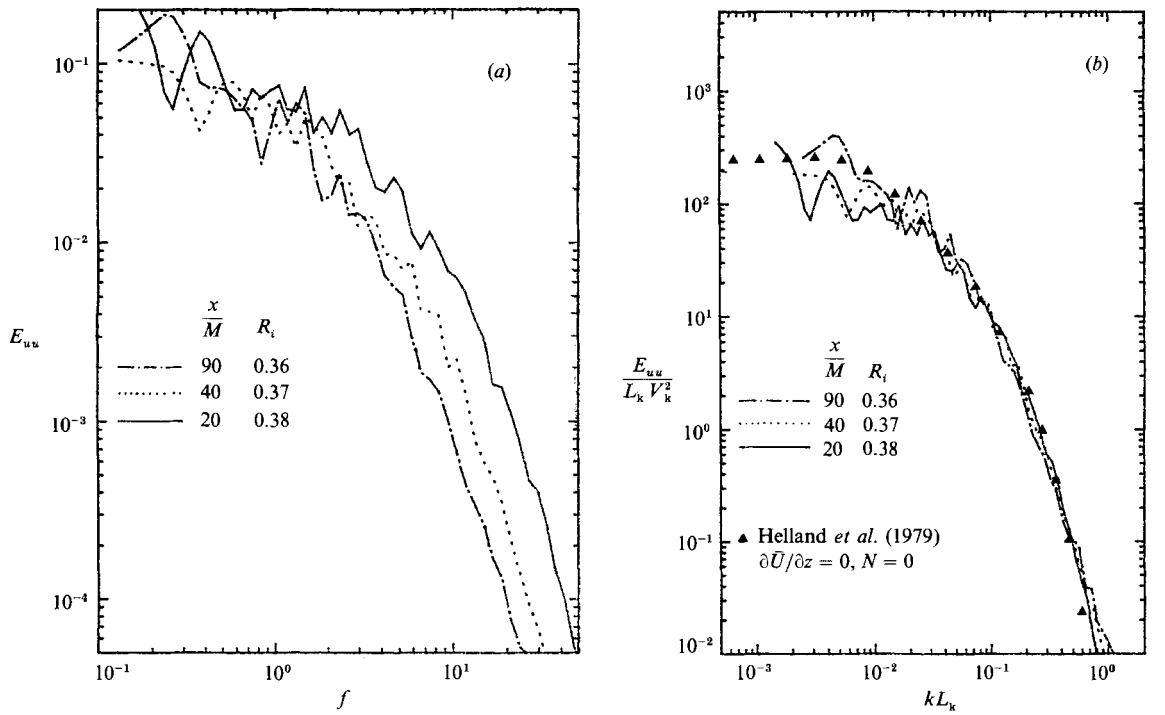

FIGURE 19. (*a*) Downstream development of one-dimensional spectra of the streamwise turbulent velocity, $R_i > R_{i_{cr}}$. (*b*) Normalized one-dimensional turbulent streamwise velocity spectra for $R_i > R_{i_{cr}}$.

a wind tunnel with a mean velocity gradient of 46.8 s^{-1} and centreline velocity of 1240 cm/s. Their temperature gradient $\partial T/\partial z$ was small enough to consider temperature as a passive scalar. The turbulent Reynolds number $(u'\lambda/\nu)$ was 160. The square symbols represent a composite of the Kolmogorov-scaled spectra appearing in Grant, Stewart & Moilliet (1962, hereinafter referred to as GSM). The higher non-dimensional wavenumber part of this spectrum is deleted because of instrumentation noise problems (see GSM). The square symbols in figure 18(*a*) are connected by a line of slope $-\frac{5}{3}$. This is possibly the most convincing data corroborating Kolmogorov's inertial-subrange universal similarity hypotheses. The Reynolds number of these oceanic measurements based on the mean flow and depth of the tidal channel is around 10^8. The data in figure 18(*a*) denoted by the solid triangles represent measurements of unstratified decaying grid turbulence taken in a wind tunnel by Helland, Lii & Rosenblatt (1977). Their grid Reynolds number $(\bar{U}M/\nu)$ is about 26000 while the turbulent Reynolds number is around 35 and independent of downstream evolution. For the stratified uniform mean shear data presented in figure 18(*a*, *b*) the grid Reynolds number is 3000 whereas the turbulent Reynolds number ranges from about 100 to 200, increasing downstream. The tendency for the present stratified-shear spectra to approach the universal-inertial-subrange spectrum is apparent as the Richardson number approaches zero. In figure 18(*b*) are some of the corresponding normalized vertical turbulent velocity spectra. The effect of the uniform mean shear on spectral growth ($R_i < R_{i_{cr}}$) is less pronounced than the preceding case (figure 18*a*) as expected from (1) and (3). Only in (1) for the streamwise component of the fluctuating kinetic energy does a shear

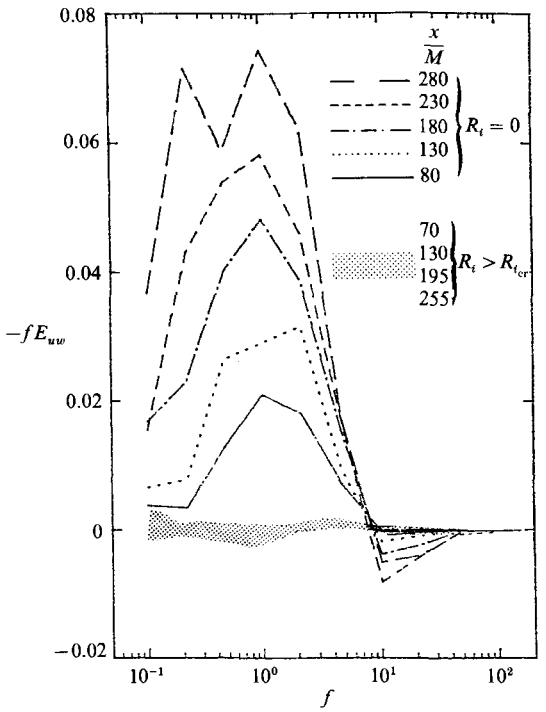

FIGURE 20. Downstream development of u, w variance-preserving cospectra for $R_i = 0$ and $R_i > R_{i_{cr}}$.

production term appear explicitly, whereas the damping effect due to stable stratification first effects the vertical component (3).

When the stability of the flow is large enough to suppress the turbulence, i.e. $R_i > R_{i_{cr}}$, the area under consecutive downstream E_{uu} spectra decreases (see figure 19*a*) as it must since $\overline{u^2}$ is now decaying. What is a little surprising is how this net decrease is distributed in frequency. The energy at low frequency is not observed to decay as does the energy at the high-frequency end of the spectra. This is reminiscent of what SHV and IHV had found in their studies of stably stratified grid decaying turbulence in a uniform mean flow. They attributed this phenomenon to the generation of internal waves. The existence of background internal waves in these particular data sets is also likely since both experiments have the same inlet conditions, and when $R_i > R_{i_{cr}}$, the shear production term is negligible compared to ϵ. The corresponding one-dimensional spectra of the vertical turbulent velocity ($R_i > R_{i_{cr}}$) are also similar to what SHV and IHV found (for the same inlet conditions), i.e. a conspicuous spectral rise at the low frequencies which persists downstream. With Kolmogorov scaling, the spectra of figure 19(*a*) can be compared to the spectra of Helland *et al.* which, as previously discussed, were taken from measurements of unstratified grid turbulence. The similarity between the spectra in figure 19(*b*) further supports the notion that when $R_i > R_{i_{cr}}$ the influence of the uniform mean shear on the dynamics of the flow is small.

The cospectrum E_{uw} measures the contribution of various frequencies to the covariance $\overline{uw}$, which appears in the turbulent-kinetic-energy equation as the source term $-\overline{uw}(\partial\bar{U}/\partial z)$ and with opposite sign in the energy equation for the mean flow kinetic energy. The term $-\overline{uw}(\partial\bar{U}/\partial z)$ is crucial to turbulent production through the

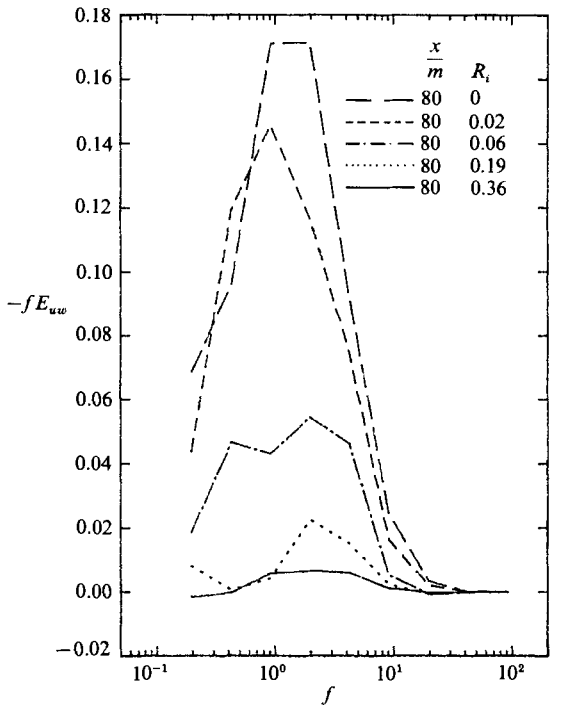

FIGURE 21. u, w variance-preserving cospectra for nearly constant $\tau (\sim 8)$ and varying R_i.

exchange of kinetic energy between the mean flow and the turbulence, with the turbulence normally profitting. In presenting the spectral form of $\overline{uw}$ it is convenient to plot $-fE_{uw}(f)$ *vs.* $\log f$ since this produces a positive covariance-preserving version of the spectra. A plot of $-fE_{uw}(f)$ *vs.* $\log f$ will give equally weighted contributions to the covariance from any portion of the plotted spectra. A similar representation is also used for the cospectrum $E_{\rho w}$. Figures 20–22 are presented in this fashion. It should be noted that measuring $\overline{uw}$ will require significantly longer (see Lumley & Panofsky 1964) averaging times than $\overline{u^2}$ and $\overline{w^2}$, for the same relative accuracy. As previously discussed, owing to limited averaging time, the covariance spectra for both $\overline{uw}$ and $\overline{\rho w}$ provide only qualitative information of general trends. The smoothed spectra were obtained by averaging neighbouring frequency bands.

Figures 20 and 21 compare the downstream evolution of the $\overline{uw}$-cospectra for flows with $R_i = 0$, $R_i < R_{i_{cr}}$, and $R_i > R_{i_{cr}}$. In the case where $R_i < R_{i_{cr}}$, the absolute values of the $\overline{uw}$-cospectra grow downstream, consistent with the increasing turbulence intensities. The lower frequencies are observed to be the largest contributors to $\overline{uw}$ and as the turbulence evolves downstream this contribution shifts towards even lower frequencies. This is believed to reflect the connection between $\overline{uw}$ and the growing integral lengthscales. The larger the average overturning eddy scale grows, because of the superimposed mean velocity gradient, the larger the streamwise fluctuations it will transport, increasing $\overline{uw}$. At high frequencies the contribution to the correlation between u and w is found to be essentially zero, as is implied by the hypothesis of local isotropy and first verified by Corrsin (1951). The argument for expecting isotropy at small scales, despite the presence of a mean shear, is that the strain field containing the smallest scales is not determined by the mean strain but by the turbulence. The ratio of the mean to turbulent strain,

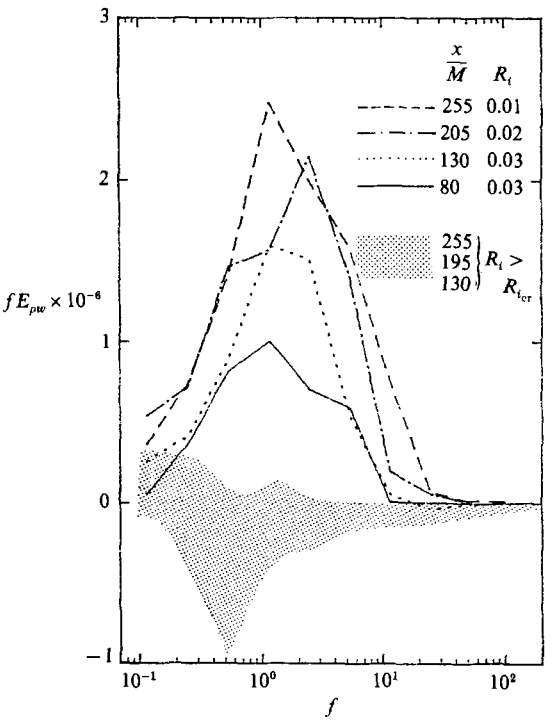

FIGURE 22. Downstream development of ρ, w variance-preserving cospectra for $R_i < R_{i_{cr}}$ and $R_i \geqslant R_{i_{cr}}$.

$(\partial \bar{U}/\partial z)/(\epsilon/\nu)^{\frac{1}{2}}$, for the growing unstratified flow of figure 20 is about 0.14. When the stratification is strong enough so that the turbulence decays, cospectral contributions to $\overline{uw}$ are found to be much smaller at all frequencies, in agreement with the observation that the largest lengthscales are now observed to decay. In figure 21 the $\overline{uw}$-cospectra are plotted for the full range of gradient Richardson numbers. Here the measurements were taken at nearly constant τ in order to isolate the effects of the changing stratification. It is clear that increasing stratification increasingly inhibits the vertical turbulent momentum transport ($\rho\overline{uw}$).

A parallel comparison can be made for the cospectra $E_{\rho w}$ of the covariance of the density and vertical velocity fluctuations, $\overline{\rho w}$. This quantity appears in the term $-\overline{\rho w}(\partial\bar{\rho}/\partial z)$, which acts as a source in the conservation equation for the mean-square concentration fluctuation. As suggested by Stewart (1969), SHV used the correlation $\overline{\rho w}$ as a diagnostic tool to distinguish turbulence from internal waves. The vertical mass flux is zero for linear internal waves because density and vertical velocity fluctuations are 90° out of phase.

As is shown in figure 22 when $R_i > R_{i_{cr}}$, $E_{\rho w}$ becomes significantly smaller than the value of $E_{\rho w}$ for $0 < R_i < R_{i_{cr}}$. The large negative excursions reflect a change in the sign of $\overline{\rho w}$ indicating counter-gradient mixing, i.e. restratification. In figure 22 the negative peak in $E_{\rho w}$ is observed at relatively low frequencies indicative of larger scales. The smaller scales have presumably become better mixed. It should be noted, however, in some of the data sets with $R_i > R_{i_{cr}}$ taken closer to the grid, substantial regions of negative $E_{\rho w}$ were observed at the higher frequencies and hence smaller scales.

Kolmogorov's universal similarity hypotheses for the turbulent velocity field may

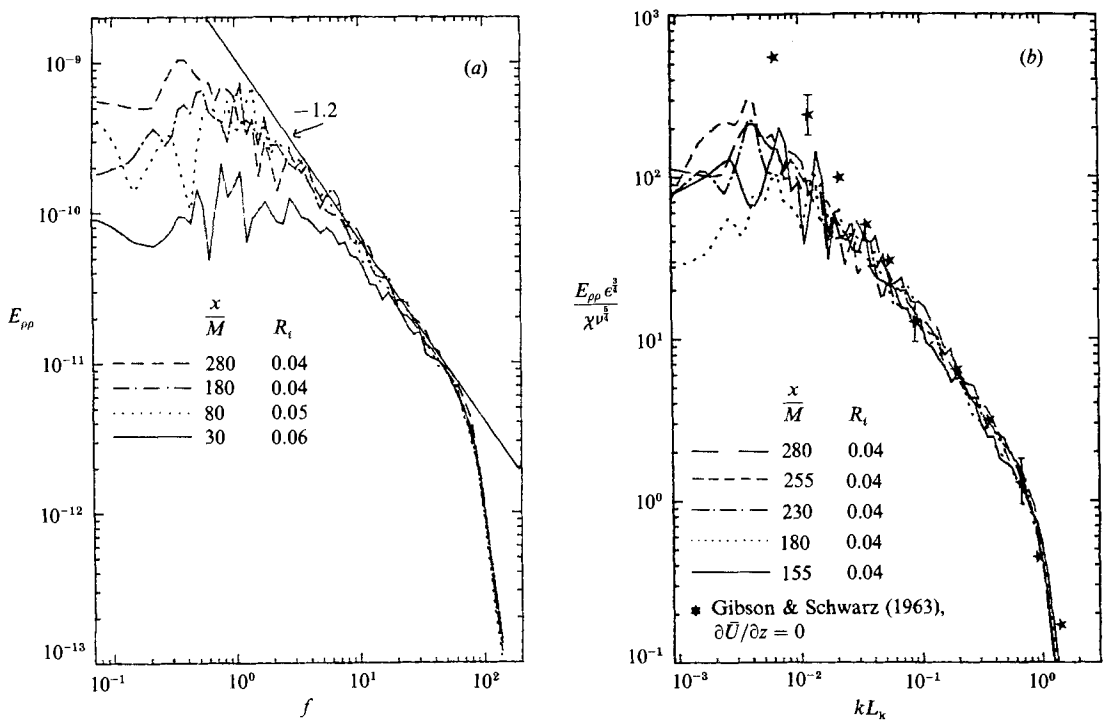

FIGURE 23. (*a*) Downstream development of one-dimensional spectra of density fluctuations for $0 < R_i < R_{i_{cr}}$. High frequencies affected by resolution of probe. (*b*) Normalized one-dimensional spectra of density fluctuations for $0 < R_i < R_{i_{cr}}$.

be extended to predict the statistical structure of conserved dynamically passive scalar fields which are mixed by the turbulence. Arguments which parallel the first similarity hypothesis lead to predictions (Batchelor 1959; Gibson 1968) about the high-wavenumber regions of the scalar spectra (viscous–convective and diffusive ranges). Unfortunately, most of these wavenumbers lie outside the spatial resolution of the conductivity probe (Head 1983). The result of extending Kolmogorov's second similarity hypothesis, which is valid only for high Reynolds number, predicts a universal scalar inertial subrange when $E_{\rho\rho}(k)\,\epsilon^{\frac{3}{4}}/(\chi\nu^{\frac{5}{4}})$ is plotted *vs.* kL_k. χ is the rate of destruction of $\overline{\rho'^2}$ by the molecular smearing of density fluctuations. Corrsin (1951) and Obukhoff (1949) independently predicted the existence of this range of k where $E_{\rho\rho}(k)$ is proportional to $k^{-\frac{5}{3}}$. As seen from the previous velocity spectra, the turbulent Reynolds number is not quite high enough to produce a broad inertial subrange. Nevertheless, there exists an intermediate range of wavenumbers comprising the viscous subrange, which may be compared using the same scaled values $E_{\rho\rho}(k)\,\epsilon^{\frac{3}{4}}/(\chi\nu^{\frac{5}{4}})$ and kL_k.

Figure 23(*a*) shows the downstream evolution of the scalar spectra $E_{\rho\rho}(k)$ in an actively stratified ($R_i \ll R_{i_{cr}}$) uniform mean shear flow. The high-wavenumber ends of the spectra are clearly attenuated by the resolution of the probe. As the influence of the mean shear extends over longer times, $E_{\rho\rho}(k)$ appears to remain proportional to $k^{-1.2}$, as seen at x/M positions of 80 to 280. This is consistent with the fact that the viscous subrange (see Gibson & Schwarz 1963), lies between the $k^{-\frac{5}{3}}$ (inertial) and k^{-1} (viscous–convective) subrange. If the corresponding slopes for the passive mixing

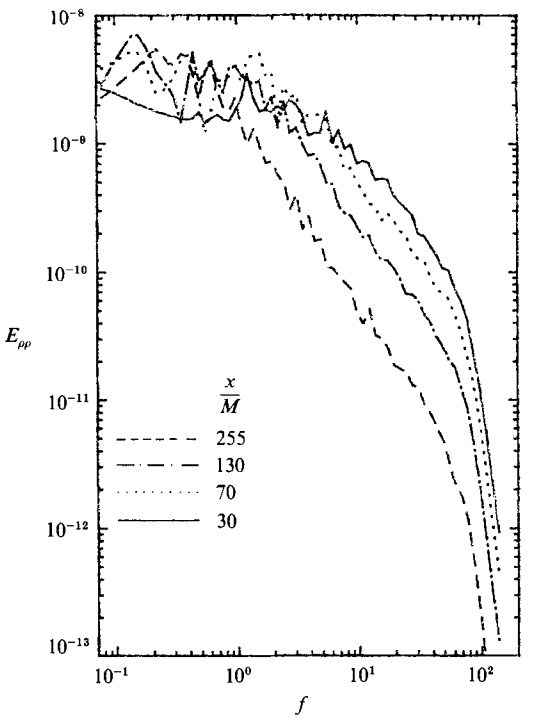

FIGURE 24. Downstream development of one-dimensional spectra of density fluctuations for $R_i > R_{i_{cr}}$.

spectra of Gibson & Schwarz (1963) and TC are calculated, then power laws of $k^{-1.23}$ and $k^{-1.21}$ are found, respectively.

The Batchelor scaling requires that χ be known. The limited spatial resolution of the conductivity probe, however, prevents direct measurements of χ. IHV estimated χ from the equation for density fluctuations, (9), which can be rewritten as

$$\chi = -\bar{U}\frac{\partial\overline{\rho^2}}{\partial x} - 2\overline{\rho w}\frac{\partial\bar{\rho}}{\partial z}. \tag{22}$$

The last term on the right-hand side of (22) was measured directly. The preceding term was estimated from a curve fit to $\overline{\rho^2}$ measured at successive downstream positions spaced 20 cm apart. For the uniform-mean shear flows, for which measurements were extended much further downstream, the measuring position intervals were spaced farther apart which discouraged estimating the spatial derivative of $\overline{\rho^2}$ with a procedure similar to IHV. Fortunately, there were some instances where $\overline{\rho^2}$ remained nearly constant, thereby allowing χ to be estimated simply as $-2\overline{\rho w}(\partial\bar{\rho}/\partial z)$.

The best estimates available for χ were from downstream measurements, $x/M =$ 155–280 for $R_i \approx 0.04$, where $\overline{\rho^2}$ varied only a few percent over this entire range. Figure 23(*b*) shows the results of applying the Batchelor scaling to these data. Also included in figure 23(*b*) are the averages of the Gibson & Schwarz (1963) normalized scalar spectra; they generated their data in a closed-loop water tunnel, in which a biplane grid that generated the velocity field also created passive-scalar fields by

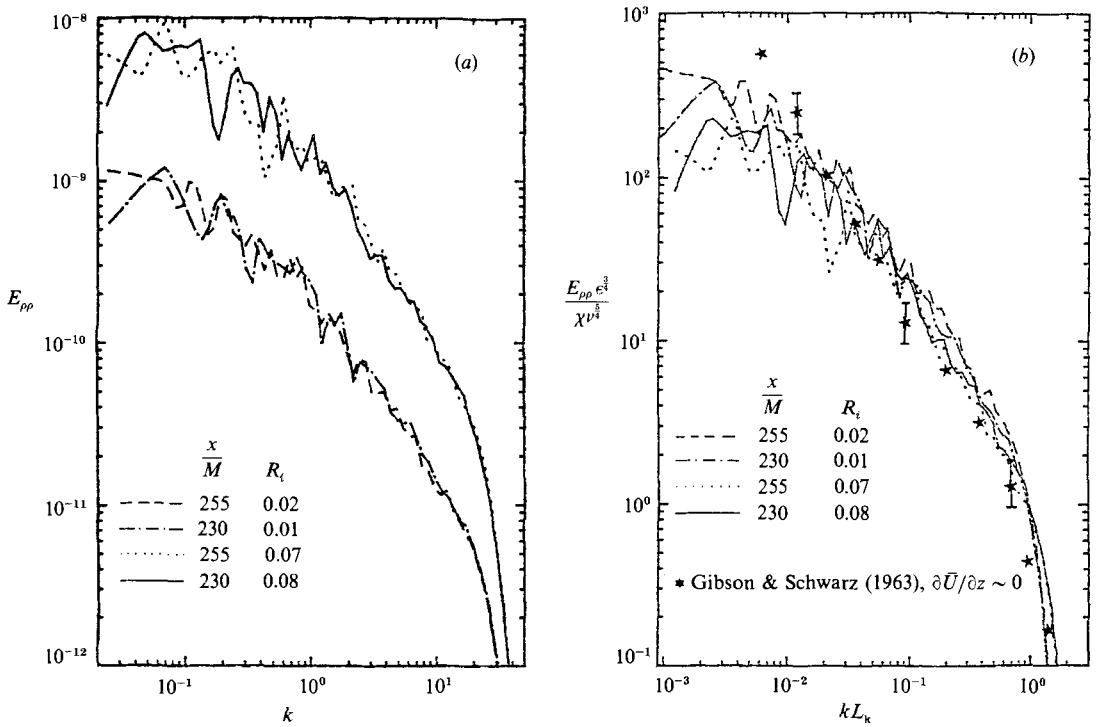

FIGURE 25. (*a*) One-dimensional spectra of density fluctuations. (*b*) Normalized one-dimensional spectra of density fluctuations.

injecting concentrated or heated salt solution through small holes drilled in the grid. The grid Reynolds number ranged from 11700 to 65550.

Figure 24 shows the evolution of $E_{\rho\rho}(k)$ when $R_i > R_{i_{cr}}$ and ρ' decreases monotonically downstream. The behaviour of the evolving $E_{\rho\rho}(k)$-spectra is similar to those found for decaying stratified grid turbulence in a uniform-mean velocity field. Again, at high frequencies the scalar spectrum is beyond the resolution of the conductivity probe.

IHV have shown that for decaying stratified grid-generated turbulence, the Batchelor scaling failed to collapse $E_{\rho\rho}(k)$-spectra taken at fixed positions far downstream of the grid but at different density gradients. However, when the Batchelor scaling was applied to either the SHV or IHV measurements taken close to the grid, a good collapse can be achieved. A good collapse close to the grid is not surprising since the Batchelor scaling is expected to work for a passive scalar and not for a strongly active scalar field. SHV had shown that for grid-generated turbulence in an actively stratified uniform mean flow, buoyancy forces are relatively small compared with inertial forces close to the grid where $L_o > L_t$. In the stratified uniform mean shear flow, where $R_i < R_{i_{cr}}$ and at large τ, L_o/L_t can become significantly greater than one, indicating that the Batchelor scaling may be appropriate. Figure 25(*a*, *b*) demonstrates how well the Batchelor scaling collapses two different stratified shear flows where $R_i < R_{i_{cr}}$, and τ are nearly the same. As discussed above, the comparison is restricted to regions of the flow where $\overline{\rho^2}$ was approximately constant.

Obviously, higher-Reynolds-number turbulent flows, better estimates of χ, and

more data at various stratifications and mean velocity gradients are needed to pursue this study further. Such studies to resolve the applicability of Batchelor scaling are further motivated by the recent high-Reynolds-number tidal-channel temperature measurements of Gargett (1985), which prompted her heretical remark that 'observations suggest that the Corrsin–Obukhov–Batchelor theory does not provide a universal description of the spectrum of temperature fluctuations in water'.

6. Comparison with and interpretation of oceanic microstructure measurements

There is naturally debate among oceanographers on how the study of laboratory turbulence can be of service towards the interpretation of oceanic microstructure (Caldwell 1983). A frequent argument made against such comparisons is that the unknown energy sources of the ocean might be quite different from the known and well-controlled energy sources of the laboratory. The approach taken here is to investigate various energy sources for turbulence in laboratory stratified flows, thereby increasing the possible comparisons that can be made with geophysical field measurements.

Some of the conclusions from the experiments of SHV are beginning to be applied in the oceanographic literature. Gregg (1984) notes that SHV's dissipation criteria for the extinction of turbulence is consistent with his own oceanic measurements. Gargett, Osborn & Nasmyth (1984), in their investigation of tidal flows over an estuary sill, used SHV's data to infer whether their unmeasured mass flux was non-zero. However, it is not known whether SHV's scenario describing the evolution of decaying grid turbulence into internal waves is generally applicable to oceanic turbulence, whose generation process is largely unidentified and highly variable in space and time. Gregg (1984) has suggested that further laboratory criteria be obtained, similar to those of SHV, but for stratified shear flows, and the present results furnish such criteria.

The value of the present uniform mean shear measurements for interpreting oceanic data will take some time to assess. Nevertheless, there are trends found in the laboratory data that encourage comparison with past field measurements. Oceanic microstructure lengthscale observations are commonly expressed in terms of the Thorpe scale L_T, defined as the root mean square of the Thorpe displacements (see Thorpe 1977). These displacements are the vertical distances individual fluid particles would have to be moved to generate a monotonic stable density profile from the observed instantaneous density profile. In the absence of internal waves or after removing their influence from the data, L_T and $L_t = \rho'/(\partial\bar{\rho}/\partial z)$ are believed to be equivalent (see Caldwell 1983; Itsweire 1984).

Figure 26(*a*) compares the overturning scale observed (L_T or L_t) with the largest possible vertical lengthscale allowed by buoyancy (L_0) for the present and SHV laboratory data, and the wind-driven mixed-layer data of Dillon (1984, Series A, B, C). Figure 26(*b*) compares the same L_t, L_T data as in (*a*) with $L_B = ((g/\bar{\rho})\overline{\rho w}/N^3)^{\frac{1}{2}}$. Dillon (1982) introduces L_B in an effort to minimize the influence of changing gradient Richardson numbers.

From figure 26(*a, b*) it is observed that when buoyancy forces are dynamically unimportant (close to the grid) neither sheared nor unsheared laboratory measurements exhibit trends similar to the oceanic data. However, when buoyancy forces dominate the dynamics of the largest scales both the unsheared and shear-flow

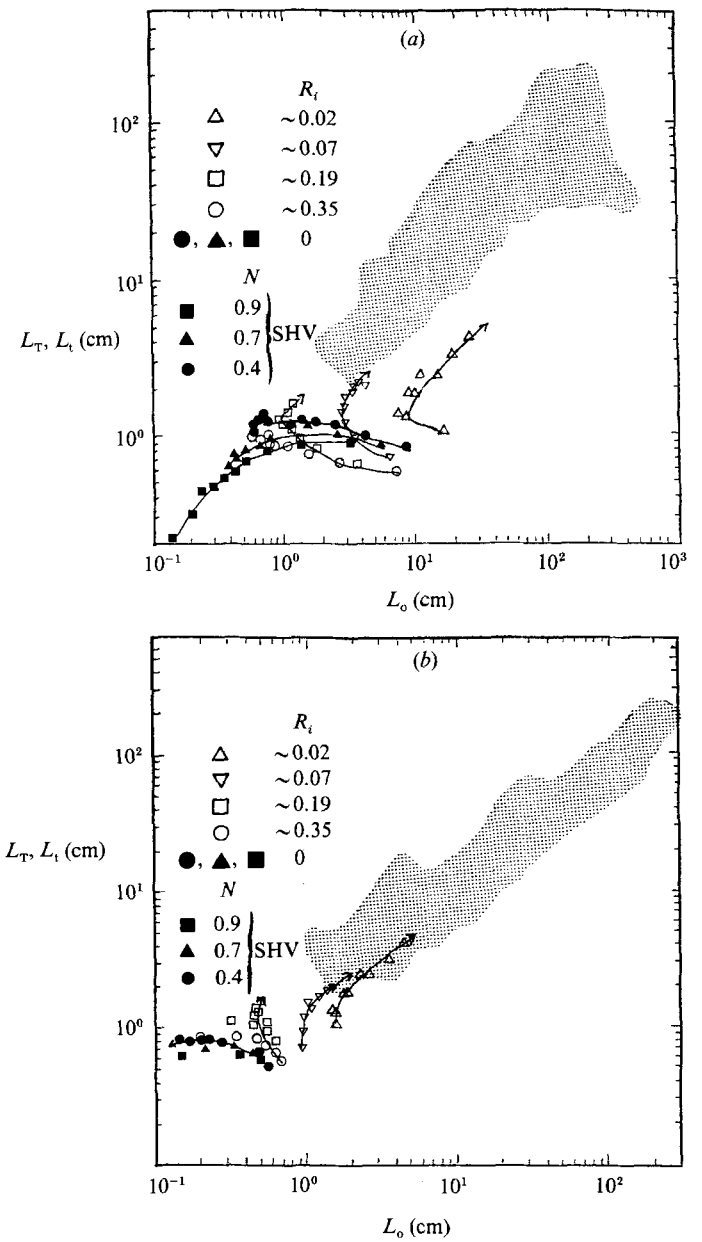

FIGURE 26. Comparison of laboratory and field lengthscale measurements. Solid symbols denote unsheared $L_t = \rho'/(\partial\rho/\partial z)$ measurements of SHV; open symbols denote present sheared measurements of L_t, ▨ denote lake measurements of L_T (Thorpe) from Dillon (1982). Arrows indicate increasing distance from grid.

data for L_T and L_o exhibit a slope and relative magnitude similar to Dillon's measurements. That is, L_T and L_o remain proportional both for the evolution of decaying ($R_i > R_{i_{cr}}$) and growing ($R_i < R_{i_{cr}}$) turbulence.

While this comparison shows that the correlation of buoyancy and overturning lengthscales found by Dillon is consistent with our observed dynamical scenarios for the evolution of buoyancy-influenced turbulence, it cannot establish in which of his

observed cases the turbulence was decaying, growing, or in a nearly steady state. Field observations in which the mean shear is also measured should allow more extensive application of the present results to interpretation of oceanographic data.

7. Concluding remarks

We have attempted to study the dominant characteristics of turbulence in a linearly stable stratified uniform-mean shear flow. In the laboratory we have approximated this flow by maintaining the region of constant mean velocity and density gradients larger than the developing lengthscale L_t. In particular we hoped to extend and refine the earlier experimental and theoretical work of Webster (1964), SHV, IHV and Tavoularis (1985).

Extending Webster's (1964) measurements further downstream from the inlet we observe that not only R_i but also τ are important parameters governing the development of stratified shear flows. By including the effects of dynamically active stable stratification in Tavoularis' (1985) approximate theory, we have obtained an equation for the turbulent kinetic energy, (17), robust enough to accommodate the broad range of behaviour that has been observed in the laboratory. When $R_i > R_{i_{cr}}$ we observe that the relation between the lengthscales L_t, L_o and L_k and the value of the transition dissipation rate (ϵ_{tr}) are similar to what SHV and IHV found for their stratified, unsheared, decaying grid-generated turbulent flow. For $R_i < R_{i_{cr}}$, unlike the uniform mean flow case of SHV and IHV, both L_t and L_o grow downstream with L_t/L_o approaching an asymptotic value that is a function of R_i.

The principal funding for this work was provided by the National Science Foundation under Grant OCE82-05946 and OCE85-11289, with partial support from DARPA Applied and Computational Mathematics Program Grant No. N00014-86-K-0758.

REFERENCES

ABARBANEL, H., HOLM, D., MARSDEN, J. & RATIU, T. 1984 Richardson number criterion for the nonlinear stability of three-dimensional stratified flow. *Phys. Lett.* **52**, 26.

BATCHELOR, G. K. 1959 Small-scale variation of convected quantities like temperature in a turbulent fluid. Part 1. General discussion and the case of small conductivity. *J. Fluid Mech.* **5**, 113.

CALDWELL, D. R. 1983 Oceanic turbulence: big bangs or continuous creation? *J. Geophys. Res.* **88**, 7543.

CHAMPAGNE, F. H., HARRIS, V. G. & CORRSIN, G. 1971 Experiments in nearly homogeneous turbulent shear flow. *J. Fluid Mech.* **41**, 81.

CORRSIN, S. 1951 On the spectrum of isotropic temperature fluctuation in an isotropic turbulence. *J. Appl. Phys.* **22**, 469.

DILLON, T. M. 1982 Vertical overturns: a comparison of Thorpe and Ozmidov length scales. *J. Geophys. Res.* **187**, 9601.

DOUGHERTY, J. P. 1961 The anisotropy of turbulence at the meteor level. *J. Atmos. Terrest. Phys.* **21**, 210.

ELGHOBASHI, S., GERZ, T. & SCHUMANN, U. 1985 Direct simulation of a turbulent homogeneous shear flow with buoyancy. In *Fifth Symp. on Turbulent Shear Flows*. Cornell University.

ELLISON, T. H. 1957 Turbulent transport of heat and momentum from an infinite rough plane. *J. Fluid Mech.* **2**, 456.

GARGETT, A. E. 1985 Evolution of scalar spectra with the decay of turbulence in a stratified fluid. *J. Fluid Mech.* **159**, 379.

GARGETT, A. E., OSBORN, T. R. & NASMYTH, P. W. 1984 Local isotropy and the decay of turbulence in a stratified fluid. *J. Fluid Mech.* **144**, 231.

GIBSON, C. H. 1968 Fine structure of scalar fields mixed by turbulence. II. Spectral theory. *Phys. Fluids* **11**, 236.

GIBSON, C. H. 1980 Fossil temperature, salinity and vorticity in the ocean. In *Marine Turbulence* (ed. J. C. T. Nihoul), p. 221. Elsevier.

GIBSON, C. H. & SCHWARZ, W. H. 1963 The universal equilibrium spectra of turbulent velocity and scalar fields. *J. Fluid Mech.* **16**, 365.

GRANT, H. L., STEWART, R. W. & MOILLIET, A. 1962 Turbulence spectra from a tidal channel. *J. Fluid Mech.* **12**, 241.

GREGG, M. C. 1984 Persistent turbulent mixing and near-inertial internal waves. In *Proc. Second 'Aha Huliko'a Hawaiian Winter Workshop* (ed. P. Muller & R. Pujalet), p. 1. Hawaii Institute of Geophysics.

HARRIS, V. G., GRAHAM, A. A. & CORRSIN, S. 1977 Further experiments in nearly homogeneous turbulent shear flow. *J. Fluid Mech.* **81**, 657.

HEAD, M. J. 1983 The use of miniature four-electrode conductivity probes for high resolution measurements of turbulent density or temperature variations in salt-stratified water flows. Ph.D. thesis, University of California, San Diego.

HELLAND, K. N., LII, K. S. & ROSENBLATT, M. 1977 Bispectra of atmospheric and wind tunnel turbulence. In *Proc. Symp. on Applications of Statistics* (ed. P. R. Krishnaiah), Vol. 2, p. 123. Academic.

ITSWEIRE, E. C. 1984 Measurements of vertical overturns in a stably stratified turbulent flow. *Phys. Fluids* **27**, 764.

ITSWEIRE, E. C., HELLAND, K. N. & VAN ATTA, C. W. 1986 The evolution of grid-generated turbulence in a stably stratified fluid. *J. Fluid Mech.* **162**, 299.

IVEY, G. N. & CORCOS, G. M. 1982 Boundary mixing in a stratified fluid. *J. Fluid Mech.* **121**, 1.

KARNIK, U. & TAVOULARIS, S. 1983 The asymptotic development of nearly homogeneous turbulent shear flow. In *Tubulent Shear Flows 4* (ed. L. J. S. Bradbury, F. Durst, B. E. Launder, F. W. Schmidt & J. H. Whitelaw), p. 14.18. Springer.

KARNIK, U. & TAVOULARIS, S. 1987 Generation and manipulation of uniform shear with the use of screens. *Exp. Fluids* **5**, 247.

KOMORI, S., UEDA, H., OGINO, F. & MIZUSHINA, T. 1983 Turbulence structure in stably stratified open-channel flow. *J. Fluid Mech.* **130**, 13.

KOOP, G. C. & BROWAND, F. K. 1979 Instability and turbulence in a stratified fluid with shear. *J. Fluid Mech.* **93**, 135.

LAUNDER, B. E. 1975 On the effects of a gravitational field on the turbulent transport of heat and momentum. *J. Fluid Mech.* **67**, 569.

LIN, J.-T. & PAO, Y.-H. 1979 Wakes in stratified fluids. *Ann. Rev. Fluid Mech.* **11**, 317.

LINDEN, P. F. 1979 Mixing in stratified fluids. *Geophys. Astrophys. Fluid Dyn.* **13**, 3.

LUMLEY, J. L. & PANOFSKY, H. A. 1964 *The Structure of Atmospheric Turbulence.* Interscience.

MILES, J. W. 1961 On the stability of heterogeneous shear flows. *J. Fluid Mech.* **68**, 577.

MONTGOMERY, R. D. 1974 An experimental study of grid turbulence in a thermally-stratified flow. Ph.D. thesis, University of Michigan.

MULHEARN, P. J. & LUXTON, R. E. 1975 The development of turbulent structure in a uniform mean shear flow. *J. Fluid Mech.* **68**, 577.

OBUKHOV, A. M. 1949 Struktura temperaturnova polia v turbulentnom potoke. *Izv. Akad. Nauk SSSR Ser. Geofiz.* **3**, 59.

OWEN, D. R. & ZIENKIEWICZ, H. K. 1957 The production of uniform shear flow in a wind tunnel. *J. Fluid Mech.* **2**, 521.

OZMIDOV, R. V. 1965 On the turbulent exchange in a stably stratified ocean. *Izv. Acad. Sci. USSR Atmos. Ocean Phys.* (Engl. Trans.) **1**, 853.

ROHR, J. J. 1985 An experimental study of evolving turbulence in uniform mean shear flows with and without stable stratification. Ph.D. thesis, University of California, San Diego.

ROHR, J. J., ITSWEIRE, E. C., HELLAND, K. N. & VAN ATTA, C. W. 1988 The investigation of the growth of turbulence in a uniform mean gradient shear flow. *J. Fluid Mech.* **187**, 1.

ROHR, J. J., ITSWEIRE, E. C. & VAN ATTA, C. W. 1984 Mixing efficiency in stably stratified decaying turbulence. *J. Geophys. Astrophys. Fluid Dyn.* **29**, 221.

ROHR, J. J. & VAN ATTA, C. W. 1987 Mixing efficiency in stably stratified growing turbulence. *J. Geophys. Res.* **92**, 5481.

ROSE, W. G. 1966 Results of an attempt to generate a homogeneous turbulent shear flow. *J. Fluid Mech.* **25**, 97.

ROSE, W. G. 1970 Interaction of grid turbulence with a uniform mean shear. *J. Fluid Mech.* **44**, 767.

STEWART, R. W. 1969 Turbulence and waves in a stratified atmosphere. *Radio Sci.* **4**, 1289.

STILLINGER, D. C. 1981 An experimental study of the transition of grid turbulence to internal waves in a salt-stratified water channel. Ph.D. thesis, University of California, San Diego.

STILLINGER, D. C. 1983 The interpretation of statistics from hot-film anemometers used in salt water flows of variable temperature and density. *J. Phys.* E: *Sci. Instrum.* **15**, 1322.

STILLINGER, D. C., HEAD, M. J., HELLAND, K. N. & VAN ATTA, C. W. 1983 A closed loop gravity-driven water channel for density-stratified shear flows. *J. Fluid Mech.* **131**, 73.

STILLINGER, D. C., HELLAND, K. N. & VAN ATTA, C. W. 1983 Experiments on the transition of homogeneous turbulence to internal waves in a stratified fluid. *J. Fluid Mech.* **131**, 91.

TAVOULARIS, S. 1985 Asymptotic laws for transversely homogeneous turbulent shear flows. *Phys. Fluids* **28**, 999.

TAVOULARIS, S. & CORRSIN, S. 1981 Experiments in nearly homogeneous turbulent shear flows with a uniform mean temperature gradient. Part 1. *J. Fluid Mech.* **104**, 311.

TENNEKES, M. & LUMLEY, J. L. 1972 *A First Course in Turbulence.* Massachusetts Institute of Technology Press.

THORPE, S. A. 1977 Turbulence and mixing in a Scottish loch. *Phil. Trans. R. Soc. Lond.* A **286**, 125.

WEBSTER, C. G. A. 1964 An experimental study of turbulence in a density-stratified shear flow. *J. Fluid Mech.* **19**, 221.